Research Square

Preprints are preliminary reports that have not undergone peer review.
They should not be considered conclusive, used to inform clinical practice,
or referenced by the media as validated information.

Multi-omics Analysis Reveals the Antioxidant Medicinal Value and Biosynthetic Mechanism of Green Fruits in Rubus chingii Hu

Xiurong Xu

1523116778@qq.com

Zhejiang Academy of Forestry

Article

Keywords: Rubus chingii Hu, antioxidant activity of green fruits, multi-omics analysis, flavonoids, RcWRKY-RcCHS/RcCHI2 regulatory pathway

Posted Date: November 20th, 2026

DOI: https://doi.org/10.21203/rs.3.rs-11400820/v1

License: This work is licensed under a Creative Commons Attribution 4.0 International License.
Read Full License

Additional Declarations: No competing interests reported.

Multi-omics Analysis Reveals the Antioxidant Medicinal Value and Biosynthetic Mechanism of Green Fruits in *Rubus chingii* Hu

Xiurong Xu*

Zhejiang Academy of Forestry, Hangzhou 310023, China

* Correspondence:

1523116778@qq.com(X.X.); Tel.: +86-0571-87798227

Keywords: *Rubus chingii* Hu; antioxidant activity of green fruits; multi-omics analysis; flavonoids; RcWRKY-RcCHS/RcCHI2 regulatory pathway

Abstract

The green fruits of *Rubus chingii* Hu possess notable antioxidant and therapeutic properties; however, their bioactive basis and regulatory mechanisms remain elusive. Here, five cultivars were evaluated using 2,2′
-azino-bis(3-ethylbenzothiazoline-6-sulfonic acid) (ABTS),
1,1-diphenyl-2-picrylhydrazyl (DPPH), and ferric reducing antioxidant power (FRAP) assays, integrated with multi-omics, network pharmacology, and molecular docking. Cultivar LR1 exhibited the highest antioxidant capacity. Metabolomics identified 3,844 metabolites, predominantly polyphenols. Weighted metabolite co-expression network analysis (WMCNA) and SwissADME (absorption, distribution, metabolism, and excretion) screening identified nine drug-like phenolic antioxidants. Network pharmacology and protein‑protein interaction (PPI) analyses revealed core targets—PTGS2, SRC, ESR1, and EGFR—enriched in redox homeostasis and cancer pathways. Transcriptomic weighted gene co-expression network analysis (WGCNA) revealed modules positively correlated with antioxidant traits and polyphenols. Key genes, including the transcription factor *RcWRKY* and structural genes encoding chalcone synthase (*RcCHS*) and chalcone isomerase (*RcCHI1*, *RcCHI2*), were significantly upregulated in LR1, validated by reverse transcription-quantitative polymerase chain reaction (RT-qPCR). Dual-luciferase reporter (Dual-LUC) and yeast one-hybrid (Y1H) assays confirmed that nuclear-localized RcWRKY directly binds to and activates the *RcCHS* and *RcCHI2* promoters. This study elucidates an RcWRKY‑RcCHS/RcCHI2‑flavonoid regulatory axis governing antioxidant biosynthesis, providing a theoretical foundation for breeding high-value medicinal cultivars.

1. Introduction

Rubus chingii Hu is a perennial shrub belonging to the genus *Rubus* in the family Rosaceae [1]. It is widely cultivated in Jiangsu, Fujian, Anhui, and Zhejiang provinces of China. In Zhejiang Province in particular, it has been included in the "New Zhejiang Eight Flavors" (*Xin Zhe Ba Wei*) list of authentic medicinal herbs and has become one of the most important berry crops under development. The mature red

fruits of *R. chingii* Hu serve as an important fruit crop, whereas the green (unripe) fruits are used medicinally [2–7]. The medicinal value of the green fruits is recorded not only in the Chinese Pharmacopoeia but also in traditional Chinese medicine, where they are recognized for their effects of tonifying the kidney, consolidating essence, nourishing the liver, and improving vision [8]. Modern pharmacological studies have demonstrated that the unripe fruits possess anticancer, anti-aging, and blood glucose-regulating properties. It has been reported that green fruit extracts can reduce postprandial blood glucose levels in mice and may be useful for the prevention and treatment of diabetes [9]. Additionally, pectic polysaccharides extracted from green fruits inhibit intestinal lipid absorption in mice, thereby exerting hypolipidemic and intestinal protective effects [10].

Oxidative damage occurs during cellular oxidative stress when the redox balance between free radical levels and cellular antioxidant defenses is disrupted. Insufficient cellular antioxidant capacity leads to the accumulation of highly toxic reactive oxygen species (ROS), which damage biological macromolecules and cause cellular and tissue injury. The ultimate consequences of oxidative damage often include various diseases, aging, and cognitive decline [11–12]. Therefore, combating oxidative damage is of great importance for modern human health. In recent years, an increasing number of traditional medicinal plants have been investigated for their potential in treating oxidative damage, with the aim of improving human redox homeostasis to treat diseases or enhance quality of life [13]. For example, ginsenoside Rc has been shown to alleviate oxidative damage and thereby improve sleep quality [14]. The extract of flower buds of *Chrysanthemum morifolium* Ramat. alleviates UVB-induced skin photoaging by enhancing antioxidant capacity [15]. Polysaccharides from *Polygonati Rhizoma* can delay cellular senescence by combating oxidative damage [16]. These studies not only demonstrate the significance of combating oxidative damage but also provide a paradigm for utilizing traditional medicinal plants. Although numerous medicinal plants have been extensively studied in relation to oxidative damage, research on *R. chingii* Hu in this regard remains limited. Investigating which specific metabolites in *R. chingii* Hu green fruits possess antioxidant functions and identifying the genes or transcription factors that regulate these antioxidant metabolites is of great significance for utilizing *R. chingii* Hu green fruits in the treatment of oxidative damage. This motivated the present study.

In recent years, metabolomics has provided a powerful tool for deciphering metabolic differences among different cultivars, laying a theoretical foundation for quality improvement [17]. In this study, metabolomics was primarily employed to elucidate the association between *R. chingii* Hu and its antioxidant activity. Due to long-term natural and artificial selection, different cultivars exhibit significant differences in quality, biotic and abiotic stress resistance, and other traits; therefore, comparing the antioxidant characteristics of multiple cultivars is more systematic and scientifically rigorous than studying a single cultivar [18–19]. Previous studies have demonstrated similar approaches: 26 key antioxidant components acting on antioxidant targets were

identified from sour jujube fruits across six production regions using metabolomics [20]; 53 potential antitumor and 52 potential anti-cardiovascular disease components were screened from four tangerine peel cultivars [21]; six metabolites targeting antioxidant-related proteins such as CDK1, EGFR, and SRC were discovered in carrots of different colors [17]; and 16 phenolic acids targeting the PI3K–AKT oxidative stress pathway were identified in strawberries from different origins [22]. These studies provide analogous methodological frameworks for identifying key antioxidant metabolites in *R. chingii* Hu.

Furthermore, this study integrates network pharmacology and molecular docking techniques to further screen for key antioxidant metabolites with drug-likeness properties and to identify their regulatory targets and associated diseases [20–22]. This research paradigm has become well established in the medical field and is gradually being extended to food science, providing new avenues for the in-depth development of medicinal and edible resources [20]. The "metabolomics + network pharmacology + molecular docking" research strategy also aligns with the modern consumer orientation toward "healthy eating." To further uncover the genes and transcription factors regulating these key antioxidant metabolites with medicinal value and drug-likeness properties in *R. chingii* Hu, transcriptomics was additionally employed. Finally, RT-qPCR, LUC, and Y1H experiments were conducted to validate the reliability of the metabolomic and transcriptomic analyses. This study also provides a theoretical basis and resource foundation for breeding *R. chingii* Hu cultivars with elevated beneficial metabolite content.

2. Results

2.1 Metabolomic Comparison of Varietal Differences and Screening of Key Antioxidant Metabolites

The antioxidant capacities of five *R. chingii* Hu cultivars were compared. In the ABTS free radical scavenging assay, LR1 exhibited the highest activity (Fig. 1A). The DPPH free radical scavenging assay indicated that LR1 had significantly higher activity than the other four cultivars (Fig. 1B). In the FRAP assay, LR1 also displayed higher activity compared to the other four cultivars (Fig. 1C). The two-dimensional PCA score plot based on the overall metabolite profiles revealed that LR1 formed a clearly independent cluster separate from the other four cultivars (Fig. 1D). OPLS-DA model prediction showed obvious discrimination between LR1 and the other four cultivars (Fig. S1A). The permutation test results showed $Q^2 > 0.9$ and $p < 0.05$, indicating that the predictive models were reliable (Fig. S1B). A total of 3,844 metabolites were identified by mass spectrometry, among which polyphenols were the most abundant class, accounting for 21.28% (Fig. 1E). Differential metabolite analysis revealed that the greatest number of differentially expressed metabolites (DEMs) was observed between LR1 and SM1, totaling 1,101 (601 upregulated and 500 downregulated), whereas the fewest DEMs were observed between LR1 and LR2, totaling 895 (555 upregulated and 340 downregulated) (Fig. 1F). Further analysis of the DEM categories revealed that polyphenols constituted the most

abundant class of DEMs between LR1 and each of the other four cultivars (Fig. 1G). To identify the most critical antioxidant capacity-related metabolites, WMCNA was performed, revealing that the blue, greenyellow, black, pink, magenta, and yellow modules were significantly positively correlated with all three antioxidant capacity indicators ($p < 0.01$) (Fig. 2A). Further analysis showed that polyphenols remained the most abundant metabolite class within these modules (Fig. 2B). To identify key antioxidant metabolites, correlations between individual polyphenols within these modules and in *vitro* antioxidant indicators were examined. A total of 75 key antioxidant metabolites were found to have correlation coefficients exceeding 0.8 with these indicators ($p < 0.05$), including 44 flavonoids, 20 phenolic acids, 5 tannins, 3 lignans, 2 stilbenes, and 1 coumarin (Fig. 2C, Table S3).

2.2 Medicinal Value Analysis of Key Antioxidant Metabolites

SwissADME evaluation identified nine phenolic metabolites with drug-likeness properties among the 75 key antioxidant metabolites. These included six flavonoids: Jmgn005927 (2-hydroxynaringenin), Lmdn006025 (2-hydroxy-2,3-dihydrogenistein), Lmdp003110 (2,6,7,4′ -tetrahydroxyisoflavanone), MWSprf104 (4′ ,6,7-trihydroxyisoflavone), MWStz329 (Isookanin), and pme0376 (Naringenin); two phenolic acids: MW0147755 (Coniferyl ferulate) and SN0308101-01 ((*S*)-4-hydroxy-5-(3,5-dihydroxyphenyl)valeric acid); and one coumarin: Lhqp101807 (Osthol). Screening through the SwissTargetPrediction and GeneCards databases revealed that these nine phenolic key antioxidant metabolites could bind to 278 oxidative damage-related targets (Fig. 3A). PPI network analysis revealed 3,477 interaction pairs among the 278 target proteins, with AKT1, EGFR, BCL2, ESR1, HIF1A, STAT3, PTGS2, SRC, HSP90AA1, and PPARG exhibiting the highest degree values (Fig. 3B). KEGG enrichment analysis of the 278 oxidative damage-related targets revealed enrichment in pathways including "Pathways in cancer," "Central carbon metabolism in cancer," "MicroRNAs in cancer," and "Alzheimer's disease," indicating that these targets are frequently associated with cancer and Alzheimer's disease (Fig. 3C). GO enrichment analysis revealed that molecular function (MF) terms were enriched in oxidoreductase activity-related pathways, which typically include both ROS-generating enzymes and antioxidant enzymes involved in ROS scavenging (Fig. 3D). Additionally, biological process (BP) terms were enriched in response to hormone and negative regulation of apoptotic process, while cellular component (CC) terms were enriched in axon and signaling receptor complex−pathways closely related to metabolic homeostasis, energy storage, and inflammatory signaling (Fig. 3D). Molecular docking of the top 10 degree-value targets with the nine key antioxidant metabolites revealed that most targets could effectively bind the key antioxidant metabolites, particularly PTGS2, SRC, ESR1, and EGFR (Fig. 3E).

2.3 Transcriptomic Comparison of Varietal Differences and Analysis of the Biosynthetic Mechanism of Key Antioxidant Polyphenol Metabolites

The two-dimensional PCA score plot based on the overall transcriptomic data revealed that the five cultivars formed clearly independent clusters (Fig. 4A). Further transcriptomic analysis was conducted to compare LR1 with the other four cultivars. DEG analysis revealed that the fewest DEGs were observed between LR1 and LR2 (3,868), while the most DEGs were observed between LR1 and SM1 (4,622) (Fig. 4B). KEGG enrichment analysis of DEGs showed that genes were predominantly enriched in "Biosynthesis of secondary metabolites" and "Metabolic pathways," with additional enrichment in "Flavonoid biosynthesis" and "Phenylpropanoid biosynthesis"−results consistent with the metabolomic analysis (Fig. 4C). WGCNA analysis revealed that the greenyellow and yellow modules were significantly positively correlated with all three antioxidant physiological indicators and the nine drug-likeness key antioxidant polyphenol metabolite contents ($p < 0.01$) (Fig. 4D). The greenyellow module contained 751 genes and the yellow module contained 1,848 genes (Fig. 4D, Table S4). Further identification revealed 15 differentially expressed transcription factors in the greenyellow module and 84 in the yellow module (Table S4). Notably, within the yellow module, LG05.1149 (RcWRKY) exhibited the highest k Within value (Table S4), indicating that RcWRKY is the hub transcription factor. Furthermore, based on the correlations between transcription factors and key antioxidant polyphenol metabolites, as well as the correlations between key antioxidant polyphenol metabolites and antioxidant physiological indicators, a significantly positively correlated network (correlation > 0.8, $p < 0.05$) was constructed (Fig. 4E). Within this network, seven transcription factors from the greenyellow module and 81 transcription factors from the yellow module promoted the biosynthesis of eight drug-likeness key antioxidant polyphenol metabolites, ultimately enhancing the three antioxidant-related indicators (Fig. 4E).

2.4 Analysis of the Mechanism by Which RcWRKY Regulates Key Antioxidant Flavonoid Biosynthesis

To gain a clearer understanding of how the hub transcription factor RcWRKY regulates key antioxidant polyphenol metabolites and thereby modulates the antioxidant medicinal value of *R. chingii* Hu, we identified LG07.1189 (a chalcone isomerase (CHI) gene family member) in the greenyellow module and LG04.4245 (a chalcone synthase (CHS) gene family member) and LG07.718 (a CHI gene family member) in the yellow module. These enzymes catalyze key upstream steps in the biosynthesis of flavanones and isoflavones in the flavonoid pathway (Fig. 5A). Moreover, the metabolites Jmgn005927 (2-hydroxynaringenin), MWStz329 (Isookanin), and pme0376 (Naringenin) are all flavanones, while Lmdn006025 (2-hydroxy-2,3-dihydrogenistein), Lmdp003110 (2,6,7,4′ -tetrahydroxyisoflavanone), and MWSprf104 (4′ ,6,7-trihydroxyisoflavone) are all isoflavones. Integration of transcriptomic and metabolomic data clearly revealed that the genes *LG07.1189*, *LG04.4245*, and *LG07.718* and the metabolites Jmgn005927, MWStz329, pme0376, Lmdn006025, Lmdp003110, and MWSprf104 were all highly expressed in LR1 (Fig. 5A). The consistent trends between gene expression and metabolite accumulation suggested that *LG07.1189*, *LG04.4245*, and *LG07.718* may

be the key biosynthetic genes regulating these metabolites (Fig. 5A). In this study, *LG07.1189*, *LG04.4245*, and *LG07.718* were designated *RcCHI1*, *RcCHS*, and *RcCHI2*, respectively. RT-qPCR experiments demonstrated that *RcWRKY*, *RcCHI1*, *RcCHS*, and *RcCHI2* were all relatively highly expressed in LR1; however, the expression trends of *RcWRKY* were more consistent with those of *RcCHS* and *RcCHI2*, which is consistent with the WGCNA transcriptomic analysis. In WGCNA, *RcWRKY*, *RcCHS*, and *RcCHI2* were all clustered in the yellow module, whereas *RcCHI1* was in the greenyellow module (Fig. 5B). Subcellular localization results showed that RcWRKY was predominantly localized in the nucleus, while RcCHS, RcCHI1, and RcCHI2 were mainly localized in the cytoplasm (Fig. 5C).

To confirm that the RcWRKY transcription factor indeed regulates the *RcCHS* and *RcCHI2* genes, LUC and Y1H assays were performed. Qualitative LUC results showed that tobacco leaves co-transformed with the RcWRKY transcription factor exhibited stronger fluorescence (Fig. 6A). Further quantitative analysis demonstrated that, compared with the empty vector control, co-transfection with the RcWRKY transcription factor resulted in a significantly higher LUC/REN ratio (Fig. 6B). To verify the reliability of the LUC assay results, Y1H validation was also performed. It was clearly observed that only yeast co-transformed with the RcWRKY transcription factor could survive on selective medium (Fig. 6C).

3. Discussion

Antioxidant physiological indicators are important criteria for evaluating the antioxidant medicinal value of plants. In this study, LR1 exhibited the highest values across all three assays−ABTS, DPPH, and FRAP−indicating that the LR1 cultivar possesses significantly superior antioxidant capacity compared to the other four cultivars. To identify the metabolites in *R. chingii* Hu that influence ABTS, DPPH, and FRAP scavenging capacities, we further conducted metabolomic analysis. We found that polyphenol metabolites in the LR1 cultivar were markedly different from those in the other four cultivars and constituted the most abundant class. Previous studies have demonstrated the critical importance of polyphenols in influencing antioxidant indicators. For example, total phenolic content during the fermentation of *Dendrobium officinale* Kimura was significantly positively correlated with ABTS and DPPH scavenging capacities [36]. Total phenolic content in extracts of *Tradescantia zebrina* prepared by different methods was significantly positively correlated with ABTS, DPPH, and FRAP indicators [37]. A comparative study of 10 flower teas from the Rosaceae family also found that increased polyphenol content led to enhanced DPPH and ABTS scavenging capacities [38]. Similarly, among 10 Rosaceae fruits, increased total polyphenol content was associated with enhanced DPPH scavenging capacity [39]. In tea, antioxidant capacity is a key quality attribute, and comparisons among multiple tea varieties have revealed that antioxidant capacity is closely related to polyphenol content [40]. WMCNA analysis also demonstrated that the modules significantly positively correlated with antioxidant physiological indicators ($p < 0.01$) −namely the blue, greenyellow, black, pink, magenta, and yellow modules−all showed

polyphenols as the most abundant metabolite class, further validating the reliability of the DEM analysis. We further identified 75 key antioxidant metabolites with correlation coefficients exceeding 0.8 with these indicators ($p < 0.05$), of which 44 were flavonoids. Previous studies have established that flavonoids are the most important antioxidant compounds among polyphenol metabolites [41]. In black wolfberry, the flavonoids kaempferol-3-*O*-rutinoside and quercetin-3-*O*-rutinoside can enhance cellular ROS scavenging capacity [42]. In *Chrysanthemum morifolium* (Jinsi Huangju), variable-temperature drying increased total flavonoid content and thereby enhanced antioxidant capacity [43]. Flavonoid compounds extracted from *Amomum tsaoko* can scavenge free radicals [44]. Both *in vivo* and *in vitro* experiments have demonstrated that flavonoids in tangerine peel are closely related to antioxidant capacity [45]. These polyphenol metabolites explain why the LR1 cultivar exhibited superior performance in antioxidant physiological indicators.

Although 75 polyphenol metabolites were significantly correlated with antioxidant physiological indicators ($p < 0.05$), whether they possess medicinal value remains uncertain. Therefore, we conducted SwissADME evaluation and confirmed that nine phenolic metabolites possess drug-likeness properties. Among these, MWStz329 (Isookanin), pme0376 (Naringenin), and Lhqp101807 (Osthol) have been previously reported to play important roles in antioxidant activities [46–48]. Prediction results indicated that these nine metabolites can bind to 278 oxidative damage-related targets. PPI network and degree value analyses identified AKT1, EGFR, BCL2, ESR1, HIF1A, STAT3, PTGS2, SRC, HSP90AA1, and PPAR γ as the most important binding targets. Molecular docking further confirmed that most targets could effectively bind the key antioxidant metabolites, particularly PTGS2, SRC, ESR1, and EGFR. Previous studies have shown that PTGS2 is an inducible enzyme whose expression can be strongly upregulated by multiple oxidative stress signaling pathways (e.g., NF- κ B, MAPK) [49]. Moreover, PTGS2-mediated prostaglandin biosynthesis is accompanied by significant ROS generation, which in turn amplifies oxidative injury to cells [49]. Activated EGFR further promotes ROS generation through the downstream PI3K/AKT pathway, forming a positive feedback loop [26]. SRC, as a non-receptor tyrosine kinase, is involved in oxidative stress-mediated signaling cascades that contribute to tissue damage [50]. These research findings collectively demonstrate that *R. chingii* Hu can combat oxidative damage through these nine phenolic metabolites. Enrichment analysis further revealed that these targets are often associated with cancer and Alzheimer's disease. Previous studies have extensively confirmed the anticancer effects of polyphenols and their therapeutic potential in Alzheimer's disease [51–53]. The present study provides a theoretical foundation for the application of polyphenols from *R. chingii* Hu in combating oxidative damage and related diseases.

Transcriptomic DEG analysis combined with KEGG enrichment analysis revealed enrichment in "Flavonoid biosynthesis" and "Phenylpropanoid biosynthesis" pathways, consistent with the metabolomic analysis results. This also provides a gene-level explanation for the superior antioxidant value of the LR1 cultivar. During

fruit maturation of *Isatis indigotica*, enhanced flavonoid gene expression was also found to promote antioxidant physiological indicators [54]. In different potato cultivars, previous studies have also identified flavonoid biosynthetic genes as key factors promoting antioxidant physiological indicators in potato tubers [55]. WGCNA analysis identified two key modules (greenyellow and yellow) that were significantly positively correlated with all three antioxidant physiological indicators and the contents of nine drug-likeness key antioxidant polyphenol metabolites ($p < 0.01$). This indicates that genes within these two modules play important roles in influencing the medicinal value of *R. chingii* Hu; therefore, subsequent analyses focused on mining key genes and transcription factors from these modules. Numerous transcription factors were identified in both the greenyellow and yellow modules. Transcription factors play crucial roles in regulating polyphenol biosynthesis. Previous studies in *R. chingii* Hu have demonstrated that RcbZIP1 and RcbZIP12 regulate flavonoid biosynthesis by modulating the *Rc4CL* gene, and RcBBX26 regulates anthocyanin biosynthesis [56‑57]. Beyond *R. chingii* Hu, numerous transcription factors have been confirmed to regulate polyphenol biosynthesis, including MYB, bHLH, and WRKY families [58]. Notably, within the yellow module, we identified the RcWRKY transcription factor, which was not only a DEG but also exhibited the highest kWithin value; therefore, we designated it as the hub transcription factor playing a critical role in regulating the entire yellow module. Analysis further revealed that the greenyellow and yellow modules contained *RcCHS*, *RcCHI1*, and *RcCHI2*−key enzymes regulating the upstream biosynthesis of flavanones and isoflavones in the flavonoid pathway. Integration of transcriptomic and metabolomic data with RT-qPCR validation confirmed that RcWRKY, RcCHS, RcCHI1, and RcCHI2 were indeed highly expressed in the LR1 cultivar, suggesting that they may indeed be the genes regulating downstream medicinally valuable flavonoid metabolites. Based on the WGCNA results showing that *RcWRKY*, *RcCHS*, and *RcCHI2* were all in the yellow module, and RT-qPCR results demonstrating more consistent expression trends among RcWRKY, RcCHS, and RcCHI2, we proposed that the RcWRKY transcription factor is more likely to regulate *RcCHS* and *RcCHI2* genes. The LUC and Y1H experiments ultimately confirmed this hypothesis. Previous studies have shown that CoWRKY28 can regulate the *CoCHS3* gene to modulate flavonoid content in *Camellia oleifera* [59]. In maize, ZmWRKY82 can regulate *ZmCHI6* to promote flavonoid biosynthesis [60]. Our study is the first to reveal the mechanism by which the RcWRKY transcription factor regulates *RcCHS* and *RcCHI2* genes to promote downstream flavonoid metabolite biosynthesis in *R. chingii* Hu.

4. Materials and Methods

4.1 Sample Collection

The experimental materials of *R. chingii* Hu were planted at the Lishui base four years ago. The cultivar names were 'Lirun No. 1', 'Lirun No. 2', 'Lifeng No. 1', 'Lifeng No. 2', and 'Shumei No. 1'. Green fruits from each cultivar were collected on May 20, 2026. The collected fruits were immediately frozen in liquid nitrogen and ground into powder for subsequent physiological indicator measurements, metabolomics,

transcriptomics, and RT-qPCR analyses. Three biological replicates were set for each cultivar.

4.2 Measurement of Physiological Indicators

4.2.1 2,2-Azinobis-3-ethylbenzothiazoline-6-sulphonate (ABTS) Free Radical Scavenging Assay

Samples were ground into powder in liquid nitrogen. Approximately 0.1 g of sample was weighed and mixed with 0.5 mL of 80% ethanol by vortexing. The mixture was centrifuged at 10,000 × g for 10 min at 4°C, and the supernatant was collected and placed on ice for measurement. A 10 μL aliquot of supernatant was added to 200 μL of ABTS working solution, gently mixed, and incubated at room temperature for 5 min. The absorbance was measured at 734 nm using a SpectraMax ABS Plus-mode microplate reader (Molecular Devices, San Jose, California, USA). Distilled water was used as the blank in place of the sample solution, and the measurement procedure was the same. The free radical scavenging rate was calculated as follows: Scavenging rate (%) = [(Abs of control − Abs of sample) / Abs of control] × 100%. Finally, a standard curve was constructed using Trolox as the standard, and the Trolox equivalent antioxidant capacity (TEAC) of the samples was calculated [23].

4.2.2 1,1-Diphenyl-2-picrylhydrazyl (DPPH) Free Radical Scavenging Assay

Samples were ground into powder in liquid nitrogen. Approximately 0.1 g of sample was weighed and mixed with 0.5 mL of 80% methanol by vortexing. The mixture was incubated in a 60°C water bath for 30 min, then centrifuged at 10,000 × g for 10 min at room temperature. A 10 μL aliquot of supernatant was added to 190 μL of 0.1 mmol/L DPPH in anhydrous ethanol solution, mixed thoroughly, and incubated at room temperature in the dark for 30 min. The absorbance was measured at 515 nm using a SpectraMax ABS Plus-mode microplate reader (Molecular Devices, San Jose, California, USA). The control tube used anhydrous ethanol in place of the DPPH solution, and the blank tube used 80% methanol in place of the supernatant. The free radical scavenging rate was calculated as follows: Scavenging rate (%) = [(Abs of blank − (Abs of sample − Abs of control)) / Abs of blank] × 100% [24]. Finally, a standard curve was constructed using Trolox as the standard, and the Trolox equivalent antioxidant capacity of the samples was calculated.

4.2.3 Ferric-Reducing Antioxidant Power (FRAP) Assay

Samples were ground into powder in liquid nitrogen. Approximately 0.1 g of sample was weighed and mixed with 0.5 mL of 80% ethanol by vortexing. The mixture was centrifuged at 10,000 rpm for 10 min at room temperature, and the supernatant was collected and placed on ice for measurement. A 6 μL aliquot of supernatant was added to 180 μL of FRAP working solution and 14 μL of double-distilled water, mixed thoroughly, and incubated for 10 min. The absorbance was measured at 593 nm using a SpectraMax ABS Plus-mode microplate reader (Molecular Devices, San Jose, California, USA). A standard curve was constructed using $FeSO_4$ as the standard, and the Fe^{2+} equivalent concentration of the samples was calculated [24].

4.3 Untargeted Metabolomic Analysis

Metabolomic profiling was performed using a widely untargeted metabolomics technique by Metware Bio Inc. (Wuhan, China), based on an ultra-high-performance liquid chromatography–tandem mass spectrometry (UPLC-MS/MS) platform.

Metabolites were extracted using a methanol–water protocol. Briefly, 30 mg of powdered sample was accurately weighed into a 1.5 mL microcentrifuge tube. Then, 1.5 mL of pre-chilled (−20°C) 70% methanol aqueous solution containing internal standards was added, and the mixture was vortexed thoroughly. After centrifugation at 12,000 rpm for 3 min at 4°C, the supernatant was collected, passed through a 0.22 μm microporous membrane filter, and the resulting filtrate was transferred to an autosampler vial for UPLC-MS/MS analysis.

Separation and identification of metabolites were performed on an integrated liquid chromatography–mass spectrometry system. Chromatographic separation was carried out using a Waters ACQUITY UPLC system equipped with an HSS T3 column (1.8 μm, 2.1 × 100 mm) maintained at 40°C. The mobile phase consisted of (A) 0.1% formic acid in water and (B) 0.1% formic acid in acetonitrile, delivered at a flow rate of 0.40 mL/min. The gradient elution program was set as follows: 0–5.0 min, 95% A → 35% A; 5.0–6.0 min, 35% A → 1% A; 1% A was held until 7.5 min; subsequently, the composition was returned to 95% A within 0.1 min and equilibrated until 10 min. The injection volume was 4 μL, and samples were injected in random order. Mass spectrometric analysis was conducted on a Sciex TripleTOF 6600 system equipped with an electrospray ionization source. The ion source parameters were set as follows: curtain gas, 35 psi; nebulizer gas, 50 psi; auxiliary heating gas, 60 psi; ion source temperature, 550°C; declustering potential, ±80 V; and ion spray voltage, ±5500/−4500 V (positive/negative mode). Data were acquired in information-dependent acquisition mode. Full-scan MS spectra were collected over *m/z* 50–1250 with an accumulation time of 200 ms. Precursor ions with a charge state of 1+ and intensity exceeding 100 cps were selected for fragmentation, with up to 12 ions monitored per cycle and isotopic peaks within 4 Da excluded. Product ion scans covered the same *m/z* range of 50–1250 with an accumulation time of 40 ms, using a collision energy of 30 ± 15 eV (positive/negative mode) and unit resolution.

The raw mass spectrometry data were converted to mzXML format using ProteoWizard. XCMS was then employed for feature extraction, alignment, and retention time correction. Features with a missing data rate >50% across experimental groups were filtered out. The remaining missing values were imputed using the *K*-nearest neighbors algorithm, and peak areas were normalized based on quality control (QC) samples to correct for instrumental response drift. Metabolite identification was performed by matching against the MetWare in-house database, public databases, and predicted spectral libraries [25]. Only high-confidence entries with a composite score >0.5 and a QC coefficient of variation (CV) <0.3 were retained. For metabolites detected in both positive and negative ion modes, the entry with the highest confidence and lowest CV was kept after merging.

Multivariate statistical analysis of the metabolomic data was performed on the MetWare Cloud platform (https://cloud.metware.cn/). First, Principal Component Analysis (PCA), an unsupervised pattern recognition method, was applied to gain a preliminary overview of the overall metabolic disparities between sample groups and the variability within each group. The PCA score plot visually illustrated the clustering and separation trends of the samples, indicating whether distinct metabolic profiles existed among the groups. The identification of differentially expressed metabolites (DEMs) was based on a combination of multivariate and univariate statistical criteria. The screening thresholds were set as follows: metabolites with a VIP score ≥ 1.0 from the OPLS-DA model and an absolute fold change (FC) ≥ 2.0 [25]. Metabolites satisfying all of the above criteria were considered statistically significant DEMs.

To identify co-expressed metabolite modules associated with antioxidant physiological traits, Weighted Metabolite Co-expression Network Analysis (WMCNA) was performed on all identified metabolites [26]. A signed, scale-free co-expression network was constructed using a soft-thresholding power determined by analyzing the network topology. Metabolites with highly similar abundance profiles across all samples were clustered into modules, with each module assigned a unique color label. A soft-thresholding power (β) of 18 was selected to achieve a scale-free topology fit index (R^2) of 0.85. During the dynamic tree cut process, the minimum module size was set to 20 and the merge cut height was set to 0.25. Subsequently, to pinpoint modules biologically relevant to antioxidant functions, module eigengenes (MEs, the first principal component representing the overall abundance pattern of each module) were calculated. Correlations between the module eigengenes and the measured antioxidant physiological indicators were analyzed. Modules exhibiting a significant positive correlation ($p < 0.01$) with antioxidant indicators were selected for further functional analysis.

4.4 Network Pharmacology Analysis

The SMILES structures of each metabolite were retrieved from the PubChem database (https://pubchem.ncbi.nlm.nih.gov/) based on their chemical names. The SwissADME database (https://swissadme.ch/) was used to evaluate whether the metabolites possessed medicinal value. The screening criteria were as follows: GI absorption classified as "High" and Drug-likeness meeting the requirements of all five rule sets (Lipinski, Ghose, Veber, Egan, and Muegge). The finally selected metabolites were uploaded to the SwissTargetPrediction database (https://swisstargetprediction.ch/) for target prediction, where targets with a probability >0 were considered potential metabolite targets [27]. Oxidative damage-related targets were predicted using the GeneCards database (https://www.genecards.org/) [28]. The metabolite targets were then compared with oxidative damage-related targets to identify common targets [28].

The identified oxidative damage-related targets of the key metabolites were uploaded to the STRING database (https://cn.string-db.org/) to predict protein–protein

interaction (PPI) networks. The interaction networks were subsequently uploaded to Cytoscape v3.10.0 for degree value analysis. The oxidative damage-related targets were also uploaded to the Metascape online platform (https://metascape.org/) for Kyoto Encyclopedia of Genes and Genomes (KEGG) and Gene Ontology (GO) functional enrichment analyses [28].

4.5 Molecular Docking

Targets with high degree values in the interaction network were selected for analysis. The 3D structures of key target proteins were obtained from the UniProt database (https://www.uniprot.org/), and the 3D structures of key metabolites were retrieved from the PubChem database (https://pubchem.ncbi.nlm.nih.gov/). Molecular docking was performed using AutoDockTools 1.5.7 to predict the binding affinity between them [28].

4.6 Transcriptomic Analysis

RNA sequencing was performed using the DNBSEQ-T7+ sequencing platform (MGI Tech, Shenzhen, China) by Metware Bio Inc. (Wuhan, China). Clean reads were aligned to the *R. chingii* Hu reference genome using HISAT2 v2.0.5 [29]. Gene expression levels were quantified with the FeatureCounts tool (http://subread.sourceforge.net/), and FPKM (Fragments Per Kilobase pair per Million mapped reads) values were calculated based on transcript lengths. Differential expression analysis was performed based on the count values of genes across samples using DESeq2 v1.4.5 for significance testing. Genes with a fold change (FC) ≥ 2.0 and a false discovery rate (FDR) < 0.05 were defined as differentially expressed genes (DEGs) [30]. KEGG enrichment analysis was performed on DEGs among cultivars, and the top 15 significantly enriched KEGG pathways were retained for heatmap visualization of gene counts.

To identify co-expressed modules associated with key antioxidant metabolites, Weighted Gene Co-expression Network Analysis (WGCNA) was performed on all identified genes [31]. An appropriate soft-thresholding power was determined by analyzing the network topology, and a signed scale-free co-expression network was constructed. Based on highly similar abundance patterns across all samples, genes were clustered into distinct modules, each assigned a unique color label. A soft-thresholding power (β) of 16 was selected to achieve a scale-free topology fit index (R^2) of 0.85. During the dynamic tree cut process, the minimum module size was set to 20 and the merge cut height was set to 0.25. Subsequently, to precisely pinpoint biological modules related to antioxidant metabolites, module eigengene values (representing the first principal component of the overall abundance pattern for each module) were calculated. Module eigengenes were correlated with the antioxidant physiological indicators as well as the nine antioxidant polyphenol metabolites with drug-likeness. Modules significantly positively correlated ($p < 0.01$) with multiple antioxidant traits were prioritized for functional analysis. Transcription factors within the modules were predicted using the PlantTFDB database

(https://planttfdb.gao-lab.org/prediction.php). The importance of transcription factors was determined based on kWithin values, with the highest kWithin value designating the hub transcription factor within the module.

4.7 RT-qPCR Assay

RNA was extracted using an RNA extraction kit (SEON, Zhangjiakou, China), and then reverse-transcribed into cDNA using a reverse transcription kit (SEON, Zhangjiakou, China). Fluorescent quantitative PCR primers were designed using the Batch q-PCR Primer Design function in TBtools software, and primers were synthesized according to the sequences listed in Table S1 [32]. The RT-qPCR was performed using TB Green Premix Ex Taq (Takara, Dalian, China), with RcActin serving as the internal reference gene. The relative expression levels of target genes were calculated using the $2^{-\Delta\Delta Ct}$ method [33].

4.8 Subcellular Localization Analysis

First-strand cDNA was synthesized using the PrimeScript™ RT reagent Kit with gDNA Eraser (Takara, Beijing, China). Cloning primers were designed using Primer6 software, and the primer sequences are listed in Table S2. The designed primers were used to amplify the open reading frames (ORFs) of *RcWRKY*, *RcCHS*, *RcCHI1*, and *RcCHI2* genes. The amplification was performed using TaKaRa LA Taq® with GC Buffer (Takara, Beijing, China). Using seamless cloning technology, the ORF sequences of *RcWRKY*, *RcCHS*, *RcCHI1*, and *RcCHI2* (with the stop codon removed) were ligated into the pAN580 vector, with GFP fused at the N-terminus. These recombinant vectors were then introduced into *Arabidopsis thaliana* protoplasts using polyethylene glycol (PEG)-mediated transformation. GFP fluorescence signals were observed under a laser confocal microscope at an excitation wavelength of 470 nm to analyze the subcellular localization of RcWRKY, RcCHS, RcCHI1, and RcCHI2 proteins [34].

4.9 Dual-Luciferase Reporter (LUC) Assay and Yeast One-Hybrid (Y1H) Assay

The ORF sequence of *RcWRKY* was ligated into the pGreenII 62-SK effector vector. Using the primers listed in Table S2, the promoter sequences (2,000 bp upstream of the ATG start codon) of *RcCHS* and *RcCHI2* were amplified by PCR. The promoter sequences of *RcCHS* and *RcCHI2* were ligated upstream of the LUC gene in the pGreenII 0800-LUC reporter vector. Both recombinant vectors were transformed into *Agrobacterium* tumefaciens strain GV3101, and tobacco leaves were infiltrated via *Agrobacterium*-mediated transformation. The infiltrated tobacco plants were cultured in darkness for 24 hours, then transferred to a 25°C constant-temperature incubator with a 16-hour light/8-hour dark photoperiod for 2 days. LUC fluorescence signals were observed using a Chemiluminescence Imaging System (Tanon 5200), and LUC and REN fluorescence activities were measured using a Dual-Luciferase Reporter Gene Assay Kit (Vazyme, DL101-01). The LUC/REN relative ratio was calculated [35].

The ORF sequence of *RcWRKY* was ligated into the pGADT7 effector vector. Using the primers listed in Table S2, the promoter sequences (2,000 bp upstream of the ATG start codon) of *RcCHS* and *RcCHI2* were amplified by PCR and cloned into the pAbAi vector to construct reporter vectors. Auto-activation testing revealed that 100 ng/mL Aureobasidin A (AbA) could effectively inhibit yeast growth. Therefore, both recombinant vectors were co-transformed into Y1H Gold yeast cells, and their interaction was observed on SD-UL selective medium supplemented with 100 ng/mL AbA [35].

4.10 Data Analysis and Visualization

Correlation analyses of physiological indicators, correlations between metabolites and physiological indicators, and correlations between key metabolites and genes were all performed on the MetWare Cloud platform (https://cloud.metware.cn/) using Pearson correlation analysis. Bar charts and significance annotations were generated using GraphPad Prism 10. For multiple comparisons following one-way ANOVA, Tukey's HSD test was applied.

5. Data Availability

All other data supporting the findings of this study are available from the corresponding author upon reasonable request. Requests for access should be directed to the lead contact, who will respond within two weeks. To maintain participant privacy and comply with ethical guidelines, certain sensitive datasets may require a formal data use agreement before release. Researchers interested in reproducing the analytical workflows can find the custom scripts and code used for statistical analysis and visualization in the Supplementary Materials section of this article.

6. Acknowledgements

The author(s) declared that financial support was received for this work and/or its publication. The authors (s) declare that they received financial support for the research and/or publication of thisarticle. This study was supported by Zhejiang Provincial ResearchInstitute Special Project (2026F1065-2-8).

7. Conflict of Interest

All financial, commercial or other relationships that might be perceived by the academic community as representing a potential conflict of interest must be disclosed. If no such relationship exists, authors will be asked to confirm the following statement:

The authors declare that the research was conducted in the absence of any commercial or financial relationships that could be construed as a potential conflict of interest.

8. Author Contributions

Conceptualization, X.X.; methodology, X.X.; software, X.X.; validation, X.X.; data curation, X.X.; writing−original draft preparation, X.X; writing−review and editing, X.X.; All authors have read and agreed to the published version of the manuscript.

9. References

[1] Chen M, Jia X, Hou D, et al. Fabrication of Rubus chingii Hu ellagitannins-loaded W/O and O/W emulsion gels: Structure, stability, in vitro digestion and *in vivo* metabolism[J]. International Journal of Biological Macromolecules, 2025, 295: 139656.

[2] Wu L, Jin Y, Chen H, et al. *Rubus chingii* Hu: ethnopharmacology, phytochemistry, quality control, functions and products[J]. Future Foods, 2024, 10: 100447.

[3] Shan C, Zhu Y, Bi H, et al. Preparation, structural characterization and health benefits of polysaccharides from *Rubus chingii* Hu: a review[J]. Frontiers in Pharmacology, 2025, 16: 1592046.

[4] Jia-Yun S, Si-Qi W, Kao-Hua L I U, et al. *Rubus chingii* Hu: An overview of botany, traditional uses, phytochemistry, and pharmacology[J]. Chinese journal of natural medicines, 2020, 18(6): 401-416.

[5] Li X, Jiang J, Chen Z, et al. Transcriptomic, proteomic and metabolomic analysis of flavonoid biosynthesis during fruit maturation in *Rubus chingii* Hu[J]. Frontiers in Plant Science, 2021, 12: 706667.

[6] Hua Y, Dai B, Luo Y, et al. Integrated analysis of multiple metabolome and transcriptome revealed the accumulation of flavonoids and associated molecular regulation mechanisms in *Rubus chingii* Hu at different developmental stages[J]. Plant Physiology and Biochemistry, 2023, 204: 108085.

[7] Chen Z, Jiang J, Shu L, et al. Combined transcriptomic and metabolic analyses reveal potential mechanism for fruit development and quality control of Chinese raspberry (*Rubus chingii* Hu)[J]. Plant Cell Reports, 2021, 40(10): 1923-1946.

[8] Xu Z, Zhang G, Chen J, et al. Role of *Rubus chingii* BBX gene family in anthocyanin accumulation during fruit ripening[J]. Frontiers in Plant Science, 2024, 15: 1427359.

[9] Jun Tan, Danshu Wang, Yu Lu, et al. Metabolic enzyme inhibitory abilities, in vivo hypoglycemic ability of palmleaf raspberry fruits extracts and identification of hypoglycemic compounds[J]. Food Science and Human Wellness, 2023, 12(4): 1232-1240.

[10] Xingxing Wang, Yupeng Liu, Yongbin Xu, et al. Structural characterization of a pectic polysaccharide from *Rubus chingii* Hu. unripe fruits and its efficacy in inhibiting intestinal lipid absorption in vivo[J]. Carbohydrate Polymers, 2025, 363: 123728.

[11] Tan B L, Norhaizan M E, Liew W P P, et al. Antioxidant and oxidative stress: a mutual interplay in age-related diseases[J]. Frontiers in pharmacology, 2018, 9: 1162.

[12] Murphy M P. How mitochondria produce reactive oxygen species[J]. Biochemical journal, 2009, 417(1): 1-13.

[13] Mao S, Liang Y, Chen Z, et al. Adaptive bioactivable nanosystems for synergistic myocardial infarction therapy using traditional pharmaceutics[J]. Bioactive Materials, 2025, 54: 648-665.

[14] Chen X, Yan X, Jing C, et al. Ginsenoside Rc maintains sleep rhythm homeostasis by alleviating oxidative stress[J]. Phytomedicine, 2025, 141: 156634.

[15] Xu S, Sun X, Zhu Z, et al. The extract of buds of Chrysanthemum morifolium

ramat alleviated UVB-induced skin photoaging by regulating MAPK and Nrf2/ARE pathways[J]. Journal of Ethnopharmacology, 2024, 332: 118352.
[16] Guan Y, Li R, Lv Z, et al. The change in structure and improvement of anti-aging effects of polysaccharides in Polygonati Rhizoma after the traditional “Nine Steaming-Nine Sun-Drying”[J]. Carbohydrate Polymers, 2026, 373: 124597.
[17] He C, Mkunga J J, Zhang D, et al. Metabolite-based color codes and antioxidant mechanisms in carrots: insights from untargeted metabolomics and bioinformatics[J]. Food Chemistry, 2025: 146637.
[18] Wang J, Hu Y, Guo D, et al. Evolution and functional divergence of glycosyltransferase genes shaped the quality and cold tolerance of tea plants[J]. The Plant Cell, 2025, 37(1): koae268.
[19] Xu N, Yu Z, Wang X, et al. Influence of natural and artificial selection on the yield differences among progeny derived from crossing between subspecies in cultivated rice[J]. New Crops, 2024, 1: 100020.
[20] Chen P, Dong S, Chu L, et al. An integrated metabolomics and network pharmacology approach to reveal the antioxidant components and mechanisms of wild jujube (Ziziphus jujuba var. spinosa) fruits across China[J]. Food Chemistry: X, 2026: 103591.
[21] Cao X, Shi K, Xu Y, et al. Integrated metabolomics and network pharmacology to reveal antioxidant mechanisms and potential pharmacological ingredients of citrus herbs[J]. Food Research International, 2023, 174: 113514.
[22] Zeng Z, Xu L, Xu J, et al. In-depth profiling of Phenolics in strawberries and their potential modulatory effects on the oxidative stress-disease Axis: Insights from UHPLC-QTOF-MS-based untargeted metabolomics, network pharmacology, and molecular docking[J]. Food Chemistry, 2025, 489: 145044.
[23] Wu J, He T, Wang Z, et al. The dynamic analysis of non-targeted metabolomics and antioxidant activity of Dendrobium officinale Kimura et Migo by the synergistic fermentation of bacteria and enzymes[J]. LWT, 2024, 203: 116354.
[24] Lim W L, Wong F C, Abd Manan F, et al. Sequential ultrasound-hot water extraction of Tradescantia zebrina leaves: optimized bioactivities with limited gastrointestinal stability[J]. Food Innovation and Advances, 2025, 5(1): 37-44.
[25] Xiao Y, Qian W, Fan S, et al. Comparative study on the differences of non-volatile and volatile compounds in ten edible flower teas: An integrated multi-omics, molecular-docking and machine-learning approach[J]. LWT, 2026: 119121.
[26] Sun Y, Zhou M, Luo L, et al. Metabolic profiles, bioactive compounds and antioxidant activity of rosehips from Xinjiang, China[J]. Lwt, 2023, 174: 114451.
[27] Li L, Wen M, Hu W, et al. Non-volatile metabolite and in vitro bioactivity differences in green, white, and black teas[J]. Food Chemistry, 2025, 477: 143580.
[28] Shen N, Wang T, Gan Q, et al. Plant flavonoids: Classification, distribution, biosynthesis, and antioxidant activity[J]. Food chemistry, 2022, 383: 132531.
[29] Du Y, Ma H, Liu Y, et al. Major quality regulation network of flavonoid synthesis governing the bioactivity of black wolfberry[J]. New Phytologist, 2024, 242(2): 558-575.

[30] Sun Y, Gao C, Wang C, et al. Metabolomics analysis reveals dynamic changes in the quality components and antioxidant activity capacity during variable temperature drying of Jinsihuangju (*Chrysanthemum morifolium*) tea[J]. Food Research International, 2026: 118915.
[31] Huang Z, Zhao Y, Yang W, et al. Preparation of flavonoids from Amomum tsaoko and evaluation of their antioxidant and α-glucosidase inhibitory activities[J]. Food Chemistry: X, 2025, 25: 102177.
[32] Wang W, Zhang J, Liu C, et al. Metabolomics combined with extraction optimization and biochemical assays revealed flavonoids and in vitro and in vivo antioxidant activity of Ponkan Chenpi[J]. Food Research International, 2026: 118324.
[33] Patel D K. Exploring the health beneficial properties of okanin and isookanin in human complications[J]. Pharmacological Research-Modern Chinese Medicine, 2024, 12: 100465.
[34] Guo J, Hu B, Wei Y, et al. Hydrogel delivering self-assembled herbal nanoparticles accelerates diabetic wound healing through mitochondrial regulation[J]. Materials Today Bio, 2025: 102417.
[35] Liu J, Wu Q, Wu Q, et al. Modulating endoplasmic reticulum stress in APP/PS1 mice by Gomisin B and Osthole in Bushen-Yizhi formula: Synergistic effects and therapeutic implications for Alzheimer's disease[J]. Phytomedicine, 2023, 119: 155023.
[36] Huang Y, Ding X, Shen Y, et al. Bletilla striata polysaccharide (BSP) promotes hair growth and suppresses oxidative stress and senescence of dermal papilla cells by inhibiting prostaglandin-endoperoxide synthase 2 (PTGS2)[J]. International Journal of Biological Macromolecules, 2026: 150149.
[37] Kalali D. The role of the matrix metalloproteinase-9 gene in tumor development and metastasis: a narrative review[J]. Global Medical Genetics, 2023, 10(02): 048-053.
[38] Parmenter B H, Thompson A S, Bondonno N P, et al. High diversity of dietary flavonoid intake is associated with a lower risk of all-cause mortality and major chronic diseases[J]. Nature food, 2025, 6(7): 668-680.
[39] Li S, Wei Y, Liang Z, et al. Review on dietary supplements as an effective improvement of Alzheimer’s disease: Focus on structures and mechanisms[J]. Food Science and Human Wellness, 2024, 13(4): 1787-1805.
[40] Wu X, Su D, Xu J, et al. Tricetin, a dietary flavonoid, alleviates neuroinflammation and promotes autophagy in alzheimer’s disease by regulating the PI3K/akt/mTOR signaling pathway[J]. Journal of Agricultural and Food Chemistry, 2025, 73(16): 9677-9689.
[41] Chen R, Geng X, Wang L, et al. Stage-resolved multi-omics links flavonoid accumulation to antioxidant capacity in Isatis indigotica fruit[J]. npj Science of Food, 2026.
[42] Xu X, Chen X, Man Q, et al. Multi-omics, network pharmacology, and molecular docking provide insights into the genetic basis, bioactive, and potential antioxidant mechanisms in potato (*Solanum tuberosum* L.) flesh[J]. Scientia Horticulturae, 2025, 345: 114148.

[43] Xu X R, Lai J X, Cheng S. Identification of the RcbZIP gene family in *Rubus chingii* and analysis of the regulation of flavonoid synthesis by RcbZIP1 and RcbZIP12[J]. Frontiers in Plant Science, 2026, 17: 1769751.
[44] Xu Z, Zhang G, Chen J, et al. Role of *Rubus chingii* BBX gene family in anthocyanin accumulation during fruit ripening[J]. Frontiers in Plant Science, 2024, 15: 1427359.
[45] Zheng X, Zhang X, Zeng F. The regulatory network composed of phytohormones, transcription factors and non-coding RNAs is involved in the flavonoids biosynthesis of fruits[J]. Horticultural Plant Journal, 2026, 12(3): 497-508.
[46] Li J, Li A, Liu S, et al. The miR5021-WRKY28-CHS3 Module Regulates Anthocyanin Biosynthesis and Resistance to Anthracnose in Camellia oleifera Peel[J]. Plant, Cell & Environment, 2026.
[47] Wang C, Wei X, Wang Y, et al. Metabolomics and transcriptomic analysis revealed the response mechanism of maize to saline-Alkali stress[J]. Plant Biotechnology Journal, 2025, 23(12): 5397-5416.
[48] Guo L, Qiao J, Zhang L, et al. Metabolome reveals high nitrogen supply decreases the antioxidant capacity of blue honeysuckle (*Lonicera caerulea* L.) by regulating flavonoids[J]. Food Chemistry, 2025, 480: 143954.
[49] Tao M, Zhang P, Wang T, et al. Identification of key quality indicators for Zigui navel orange varieties through multivariate analyses[J]. Food Chemistry: X, 2026: 103702.
[50] Sun P, Ge G, Sun L, et al. Metabolomics combined with physiology and transcriptomics reveal the regulation of key nitrogen metabolic pathways in alfalfa by foliar spraying with nano-selenium[J]. Journal of Nanobiotechnology, 2025, 23(1): 7.
[51] Zhou L, She J, Li Q, et al. Integrated multi-omics and network pharmacology reveals antioxidant-active metabolites and health benefits of Camellia oleifera seed oil[J]. Food Chemistry, 2025: 146913.
[52] Yang Y, Cheng Z, Yang J, et al. Exploring Potential Anti-Gastric Mechanisms of Rhizoma Paridis through Integrated Computational and Experimental Analyses[J]. Phytomedicine, 2026: 158588.
[53] Guo X, Chen X, Zeng M, et al. Revealing key antioxidant compounds and mechanisms in Fritillaria Bulbus by metabolomics and network pharmacology[J]. npj Science of Food, 2025, 9(1): 124.
[54] Wang L, Lei T, Han G, et al. The chromosome-scale reference genome of *Rubus chingii* Hu provides insight into the biosynthetic pathway of hydrolyzable tannins[J]. The Plant Journal, 2021, 107(5): 1466-1477.
[55] Bai Y, Zhu M, Du B, et al. Multi-omics analyses unveil the molecular mechanism involving flavonoid-mediated color changes of different mango varieties[J]. Food Chemistry, 2025: 147663.
[56] Wang R, Shu P, Zhang C, et al. Integrative analyses of metabolome and genome-wide transcriptome reveal the regulatory network governing flavor formation in kiwifruit (Actinidia chinensis)[J]. New phytologist, 2022, 233(1): 373-389.
[57] Chen C, Wu Y, Li J, et al. TBtools-II: A “one for all, all for one” bioinformatics platform for biological big-data mining[J]. Molecular plant, 2023, 16(11): 1733-1742.

[58] Livak K J, Schmittgen T D. Analysis of relative gene expression data using real-time quantitative PCR and the $2^{-\Delta\Delta CT}$ method[J]. methods, 2001, 25(4): 402-408.
[59] Yoo SD, Cho YH, Sheen J. Arabidopsis mesophyll protoplasts: a versatile cell system for transient gene expression analysis. Nat Protoc. 2007;2(7):1565-1572. doi:10.1038/nprot.2007.199.
[60] Yang Y, Wang X, Liu J, et al. Identification and role of CmLhcb2. 1 in regulating low-light stress resistance in Chinese chestnut (*Castanea mollissima*)[J]. Frontiers in Plant Science, 2025, 16: 1552618.

Figure 1. Antioxidant capacity and metabolomic profiling of *Rubus chingii* Hu fruits across developmental stages.
(A) ABTS radical scavenging activity. (B) DPPH radical scavenging activity. (C) Ferric reducing antioxidant power (FRAP). Values are presented as the mean ± SD (n = 3); distinct lowercase letters denote statistically significant differences ($P < 0.05$, one-way ANOVA followed by Tukey's test). (D) Two-dimensional principal component analysis (2D PCA) score plot of metabolite profiles across developmental stages. (E) Doughnut chart illustrating the chemical classification and proportional distribution of the 3,844 identified metabolites. (F) Numbers of significantly upregulated and downregulated differentially expressed metabolites (DEMs) across pairwise comparisons. (G) Stacked bar chart showing the composition and distribution of metabolite classes among DEMs across different comparisons.

Figure 2. Weighted gene co-expression network analysis (WGCNA) and metabolite–trait correlation network.
(A) Module–trait relationship heatmap between co-expression modules and antioxidant indices. The color scale ranges from blue ($r = -1$) to red ($r = 1$), with corresponding P-values in parentheses. Numbers alongside module labels indicate the metabolite count per module. (B) Stacked bar chart showing the breakdown of metabolite classifications within each co-expression module. (C) Correlation network visualizing associations between antioxidant parameters (ABTS, DPPH, and FRAP) and representative metabolites (flavonoids, phenolic acids, and coumarins). Edge thickness reflects the magnitude of the correlation coefficient.

Figure 3. Regulatory network architecture and functional enrichment of core candidate genes.
(A) Transcriptional regulatory network depicting interactions between candidate transcription factors and target structural genes. (B) Co-expression network topology; node colors reflect degree centrality, with darker hues indicating higher network connectivity. (C) KEGG pathway enrichment bubble plot of core DEGs. The x-axis represents the rich factor, and the y-axis indicates enriched pathways. Bubble size corresponds to gene count, and bubble color indicates the $-\log10(P\text{-value})$. (D) Gene Ontology (GO) enrichment bubble plot categorized into Molecular Function (MF), Biological Process (BP), and Cellular Component (CC). (E) Expression correlation heatmap between key candidate genes and putative pharmacological/antioxidant

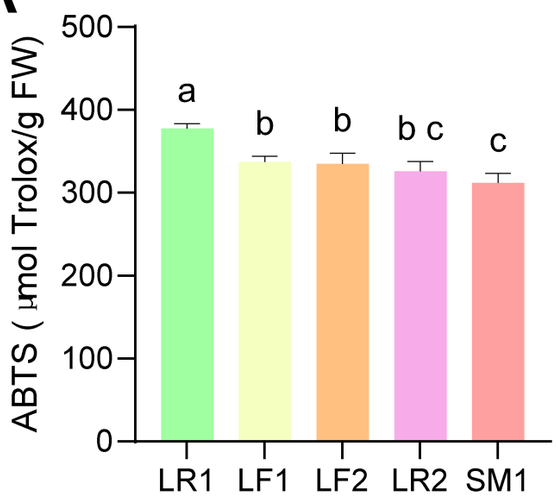
targets (e.g., AKT1, EGFR, and BCL2).

Figure 4. Transcriptomic landscapes and multi-omics integration.
(A) 2D PCA score plot of transcriptome datasets across developmental stages. (B) Counts of upregulated and downregulated DEGs across pairwise comparisons. (C) Enrichment heatmap of representative KEGG pathways across comparisons. (D) Heatmap of module–trait correlations evaluating transcriptomic modules against antioxidant traits and key metabolite classes. (E) Multi-omics co-regulatory network linking structural genes, transcription factors, metabolites (flavonoids, phenolic acids, and coumarins), and antioxidant capacities within the greenyellow and yellow modules.

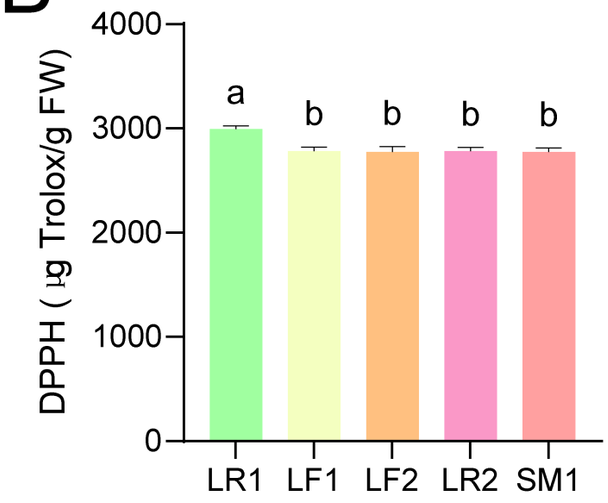
Figure 5. Phenylpropanoid pathway schematic, candidate gene expression profiles, and subcellular localization.
(A) Schematic diagram of the phenylpropanoid biosynthetic pathway. Accompanying heatmaps display transcript abundance and metabolite accumulation across developmental stages. (B) Relative expression levels of core candidate genes (*RcWRKY*, *RcCHS*, *RcCHI1*, *and RcCHI2*) across fruit developmental stages determined by qRT-PCR. Values represent the mean ± SD (n = 3); different lowercase letters indicate significant differences ($P < 0.05$, one-way ANOVA followed by Tukey's test). (C) Subcellular localization of GFP, RcWRKY-GFP, RcCHS-GFP, RcCHI1-GFP, and RcCHI2-GFP fusion proteins in plant cells. Panels from left to right: GFP fluorescence, chlorophyll autofluorescence, bright field, and merged images. Scale bar = 10 μm.

Figure 6. Transcriptional activation of *RcCHS* and *RcCHI2* promoters by RcWRKY.
(A) Representative bioluminescence imaging of dual-luciferase reporter assays. Left panels: empty vector negative controls; right panels: co-expression of the 35S::RcWRKY effector with proRcCHS::LUC or proRcCHI2::LUC reporters. (B) Quantitative analysis of relative LUC/REN enzymatic activity ratios. Data represent the mean ± SD (n = 3); different lowercase letters denote statistically significant differences ($P < 0.05$, one-way ANOVA followed by Tukey's test). (C) Yeast one-hybrid (Y1H) validation of RcWRKY binding to the *proRcCHS* and *proRcCHI2* promoter regions. Left panel: non-selective control medium (SD/−Ura/−Leu); right panel: selective screening medium (SD/−Ura/−Leu) supplemented with 100 ng/mL Aureobasidin A (AbA).

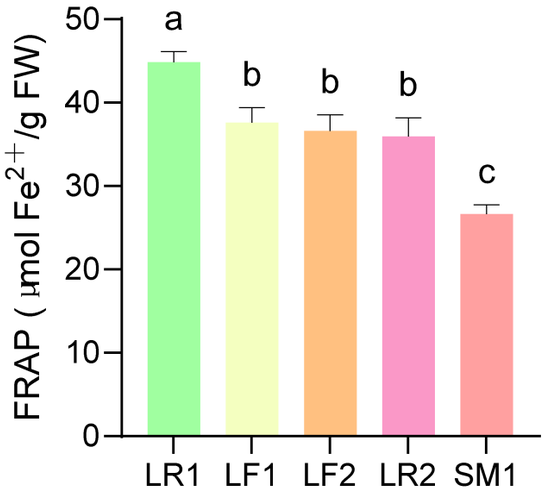
A


ABTS (μmol Trolox/g FW)
500
400
300
200
100
0
a
b
b
b c
c
LR1
LF1
LF2
LR2
SM1

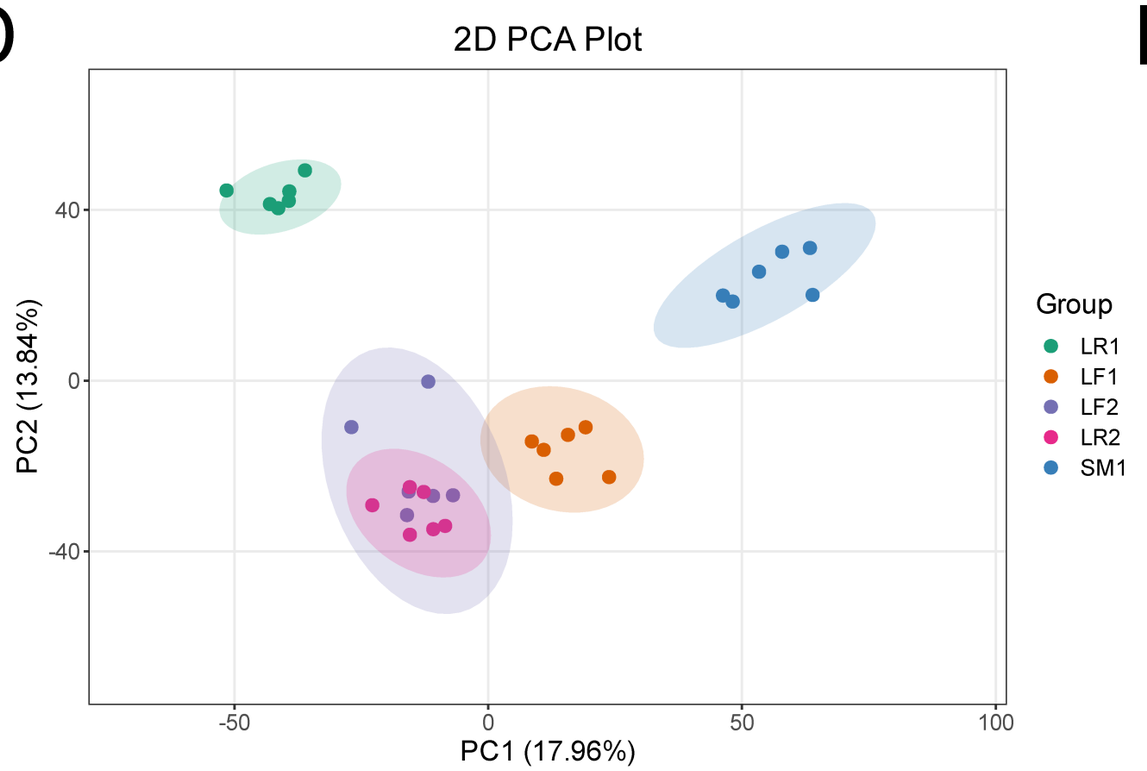
B


DPPH (μg Trolox/g FW)
4000
3000
2000
1000
0
a
b
b
b
b
LR1
LF1
LF2
LR2
SM1

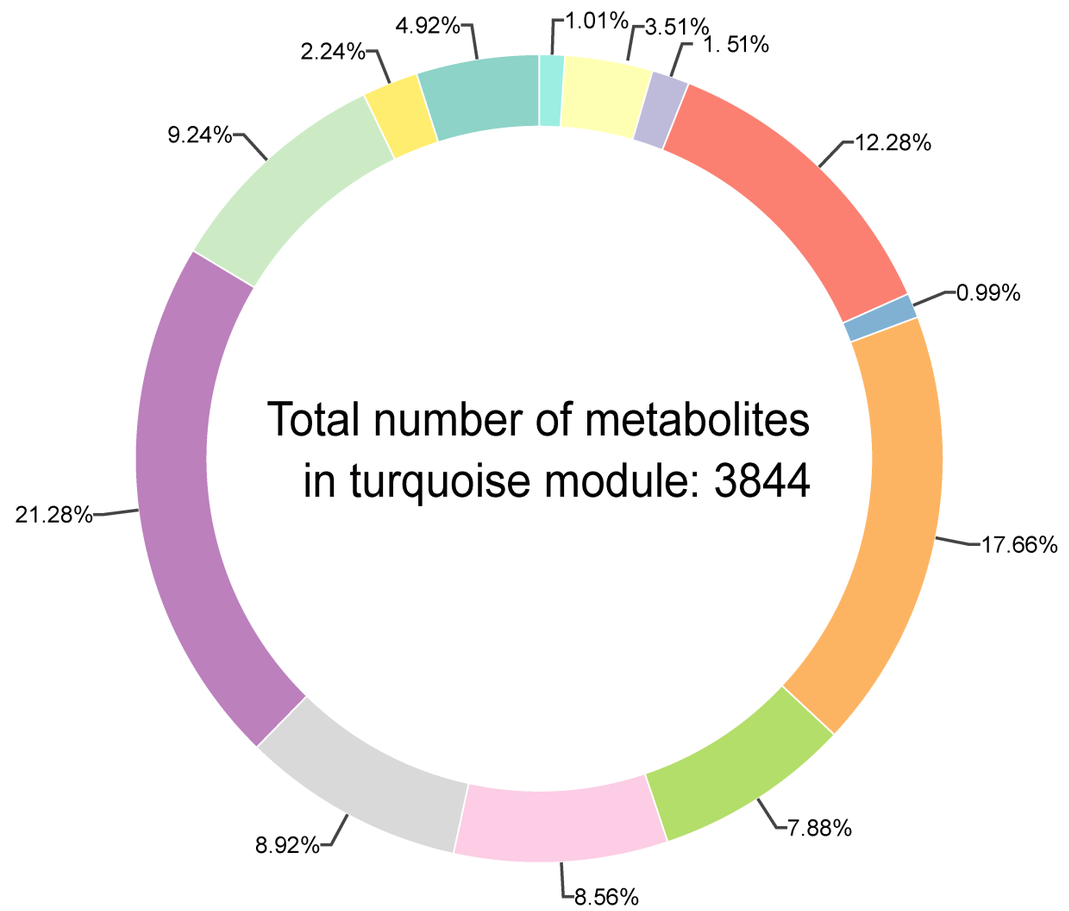
C


FRAP (μmol Fe2+/g FW)
50
40
30
20
10
0
a
b
b
b
c
LR1
LF1
LF2
LR2
SM1

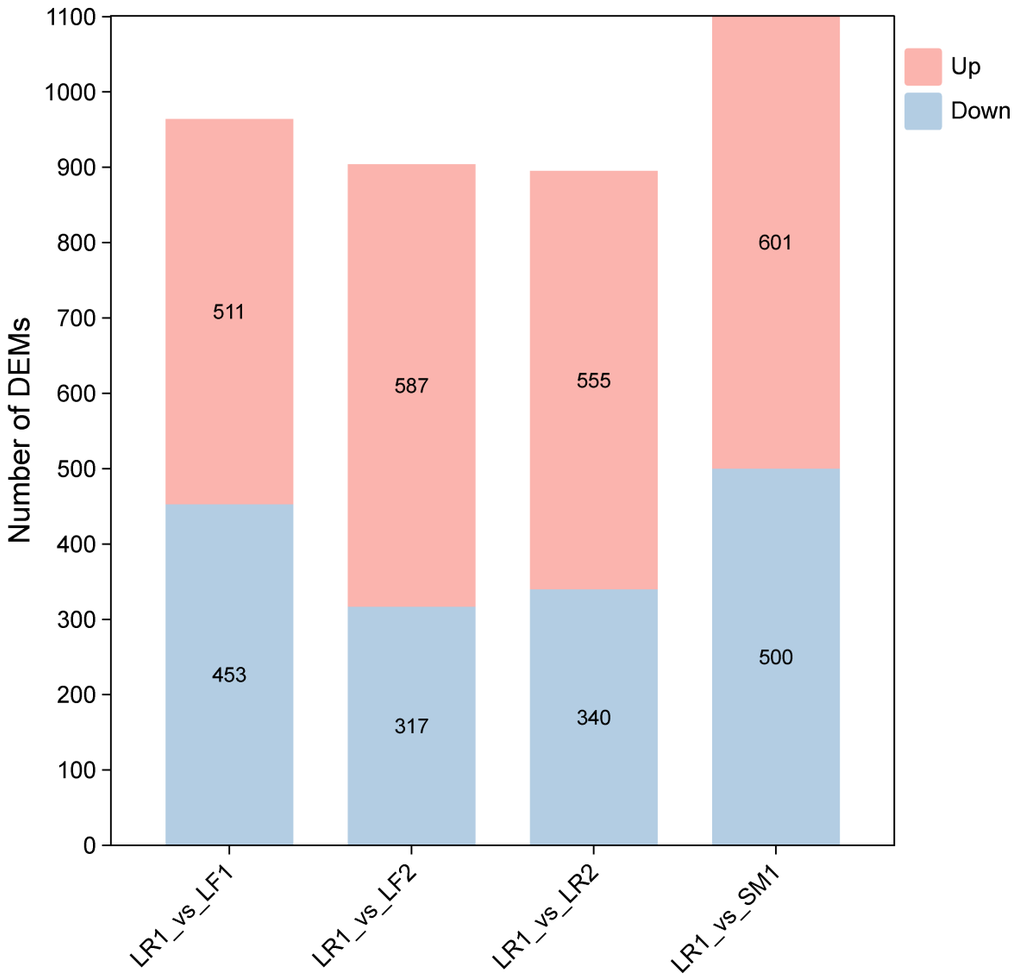
D


2D PCA Plot
PC2 (13.84%)
40
0
-40
-50
0
50
100
PC1 (17.96%)
Group
LR1
LF1
LF2
LR2
SM1

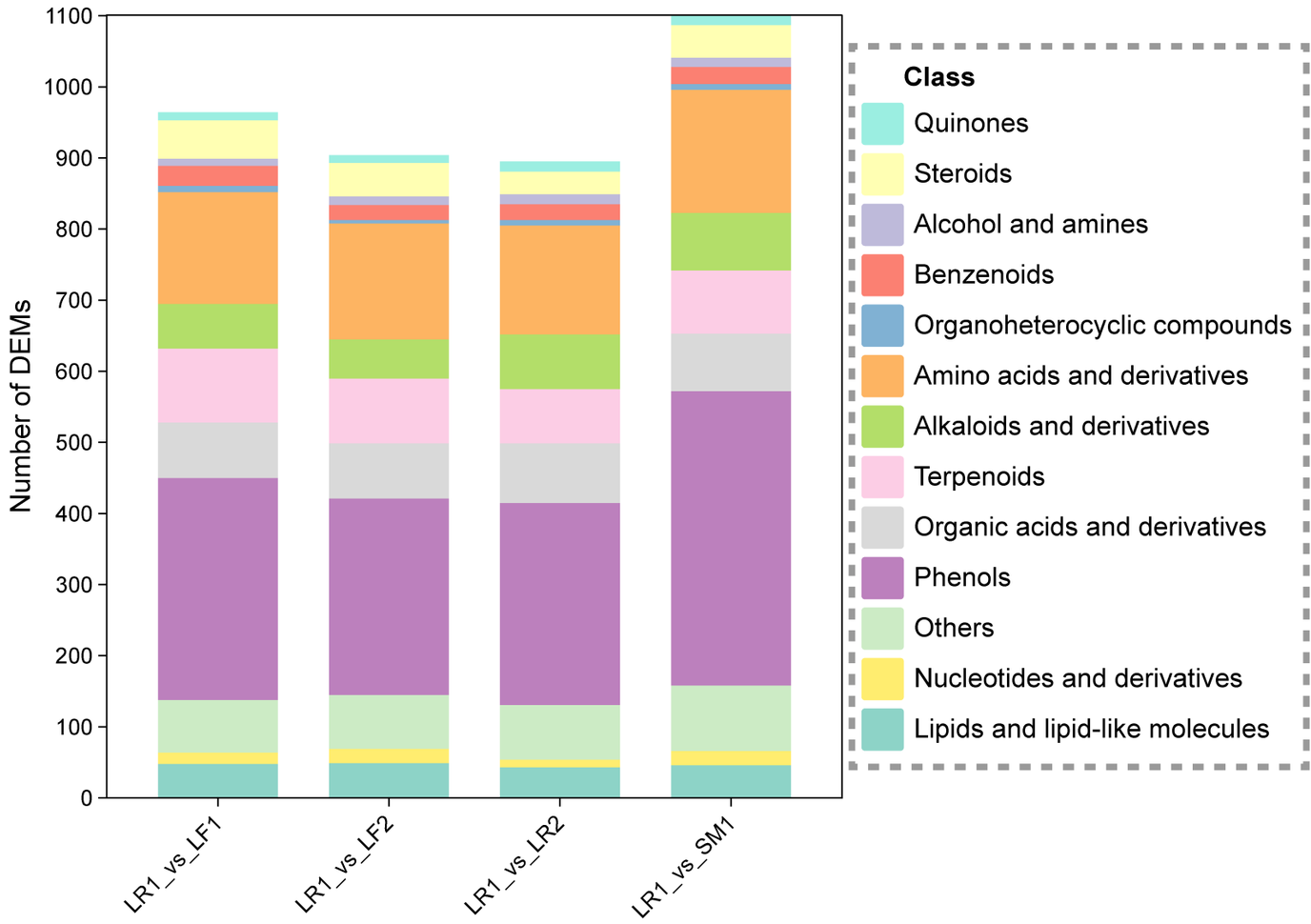
E


Total number of metabolites
in turquoise module: 3844
2.24%
4.92%
1.01%
3.51%
1. 51%
9.24%
12.28%
0.99%
21.28%
17.66%
7.88%
8.92%
8.56%

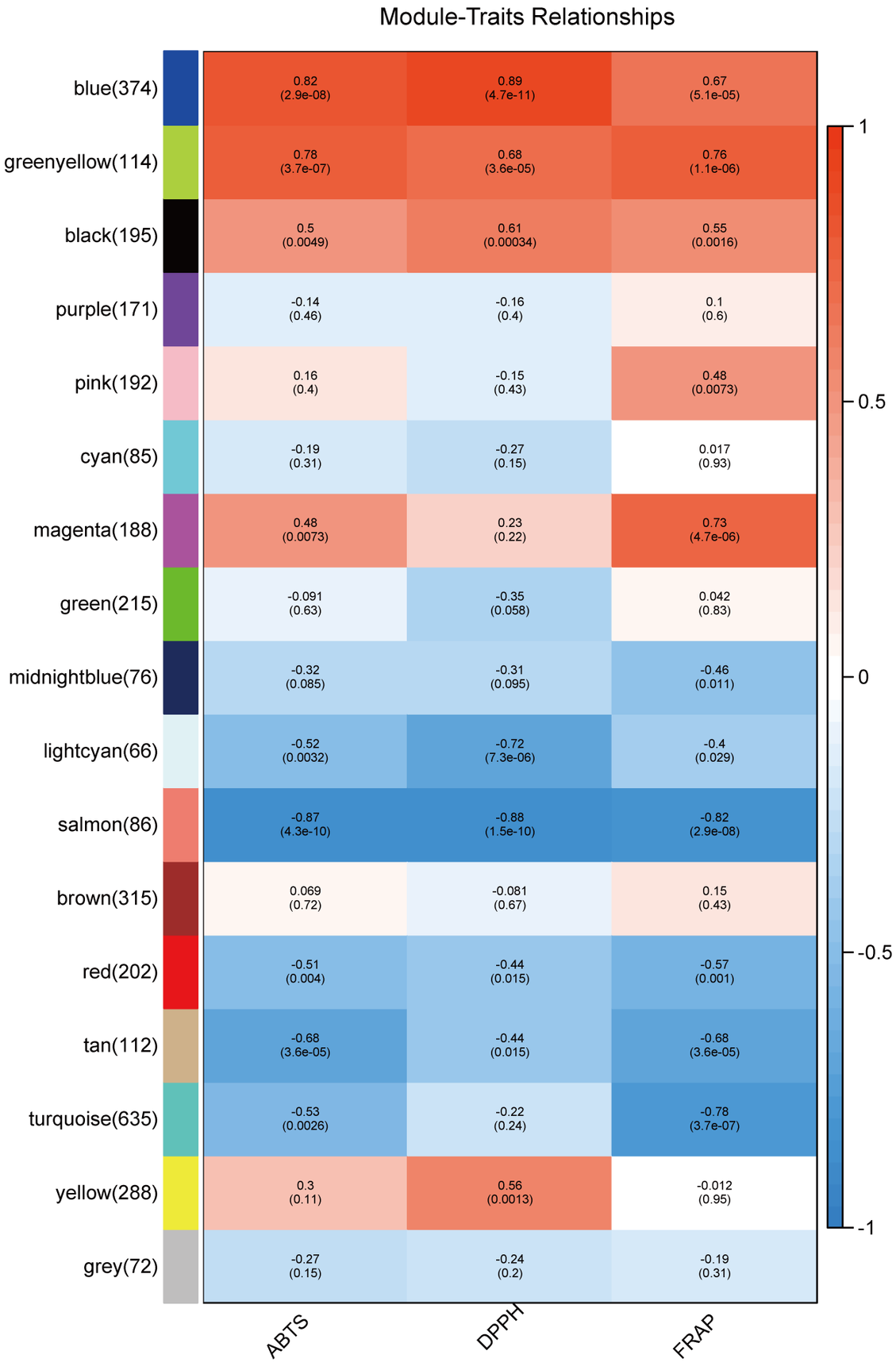
F


Number of DEMs
1100
1000
900
800
700
600
500
400
300
200
100
0
511
453
587
317
555
340
601
500
Up
Down
LR1_vs_LF1
LR1_vs_LF2
LR1_vs_LR2
LR1_vs_SM1

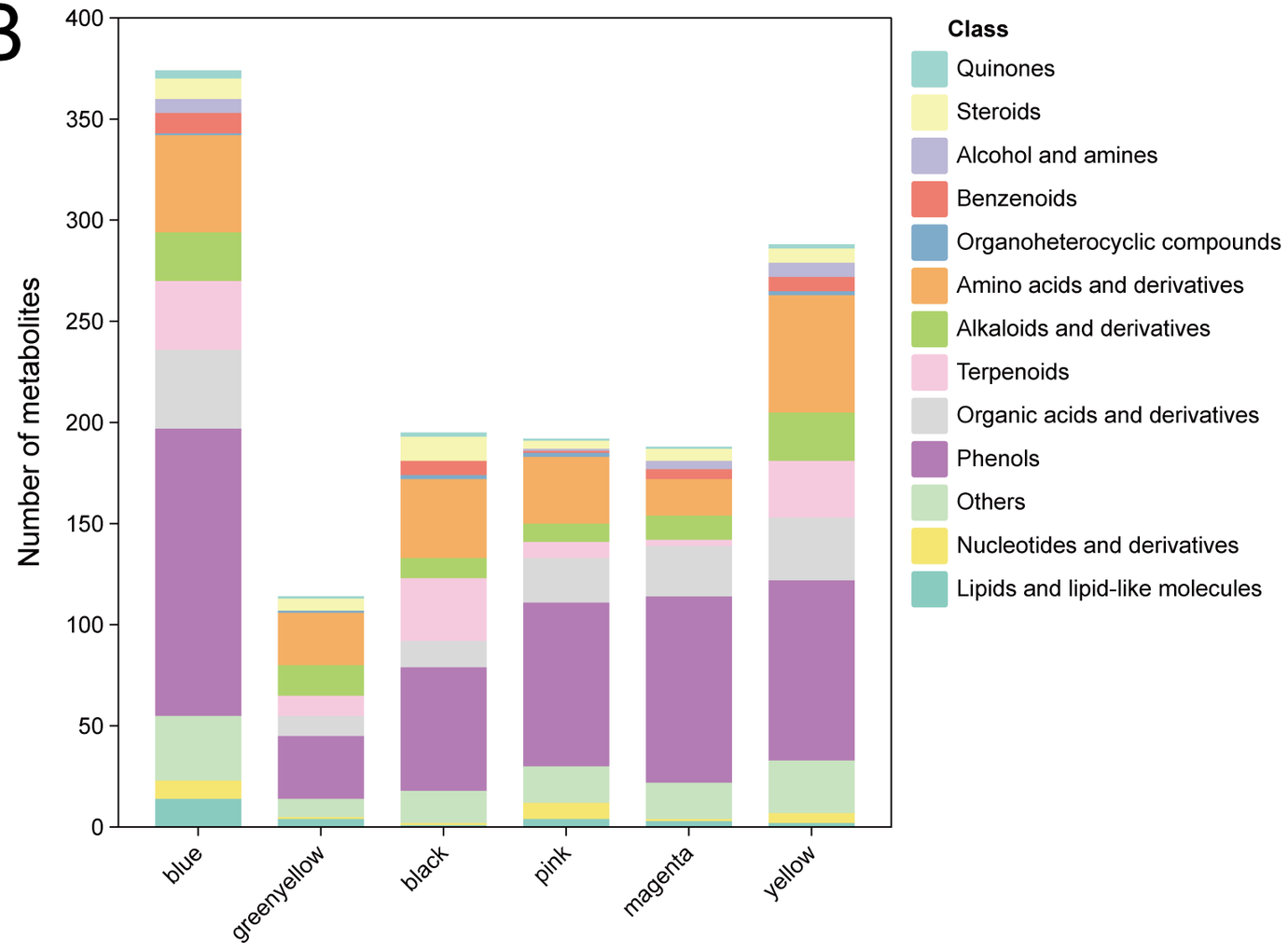
G


Number of DEMs
1100
1000
900
800
700
600
500
400
300
200
100
0
LR1_vs_LF1
LR1_vs_LF2
LR1_vs_LR2
LR1_vs_SM1
Class
Quinones
Steroids
Alcohol and amines
Benzenoids
Organoheterocyclic compounds
Amino acids and derivatives
Alkaloids and derivatives
Terpenoids
Organic acids and derivatives
Phenols
Others
Nucleotides and derivatives
Lipids and lipid-like molecules

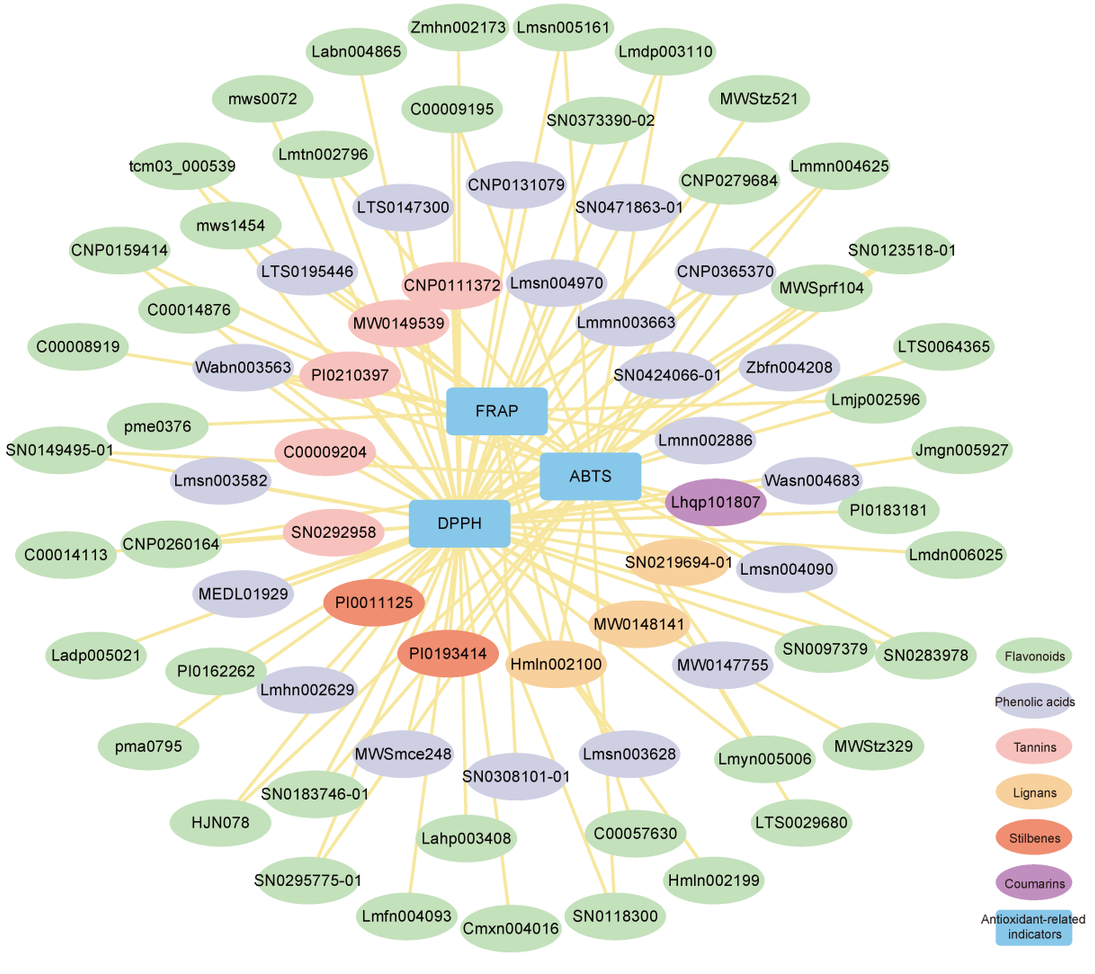
A


Module-Traits Relationships
blue(374)
greenyellow(114)
black(195)
purple(171)
pink(192)
cyan(85)
magenta(188)
green(215)
midnightblue(76)
lightcyan(66)
salmon(86)
brown(315)
red(202)
tan(112)
turquoise(635)
yellow(288)
grey(72)
0.82 (2.9e-08)
0.89 (4.7e-11)
0.67 (5.1e-05)
0.78 (3.7e-07)
0.68 (3.6e-05)
0.76 (1.1e-06)
0.5 (0.0049)
0.61 (0.00034)
0.55 (0.0016)
-0.14 (0.46)
-0.16 (0.4)
0.1 (0.6)
0.16 (0.4)
-0.15 (0.43)
0.48 (0.0073)
-0.19 (0.31)
-0.27 (0.15)
0.017 (0.93)
0.48 (0.0073)
0.23 (0.22)
0.73 (4.7e-06)
-0.091 (0.63)
-0.35 (0.058)
0.042 (0.83)
-0.32 (0.085)
-0.31 (0.095)
-0.46 (0.011)
-0.52 (0.0032)
-0.72 (7.3e-06)
-0.4 (0.029)
-0.87 (4.3e-10)
-0.88 (1.5e-10)
-0.82 (2.9e-08)
0.069 (0.72)
-0.081 (0.67)
0.15 (0.43)
-0.51 (0.004)
-0.44 (0.015)
-0.57 (0.001)
-0.68 (3.6e-05)
-0.44 (0.015)
-0.68 (3.6e-05)
-0.53 (0.0026)
-0.22 (0.24)
-0.78 (3.7e-07)
0.3 (0.11)
0.56 (0.0013)
-0.012 (0.95)
-0.27 (0.15)
-0.24 (0.2)
-0.19 (0.31)
ABTS
DPPH
FRAP
1
0.5
0
-0.5
-1

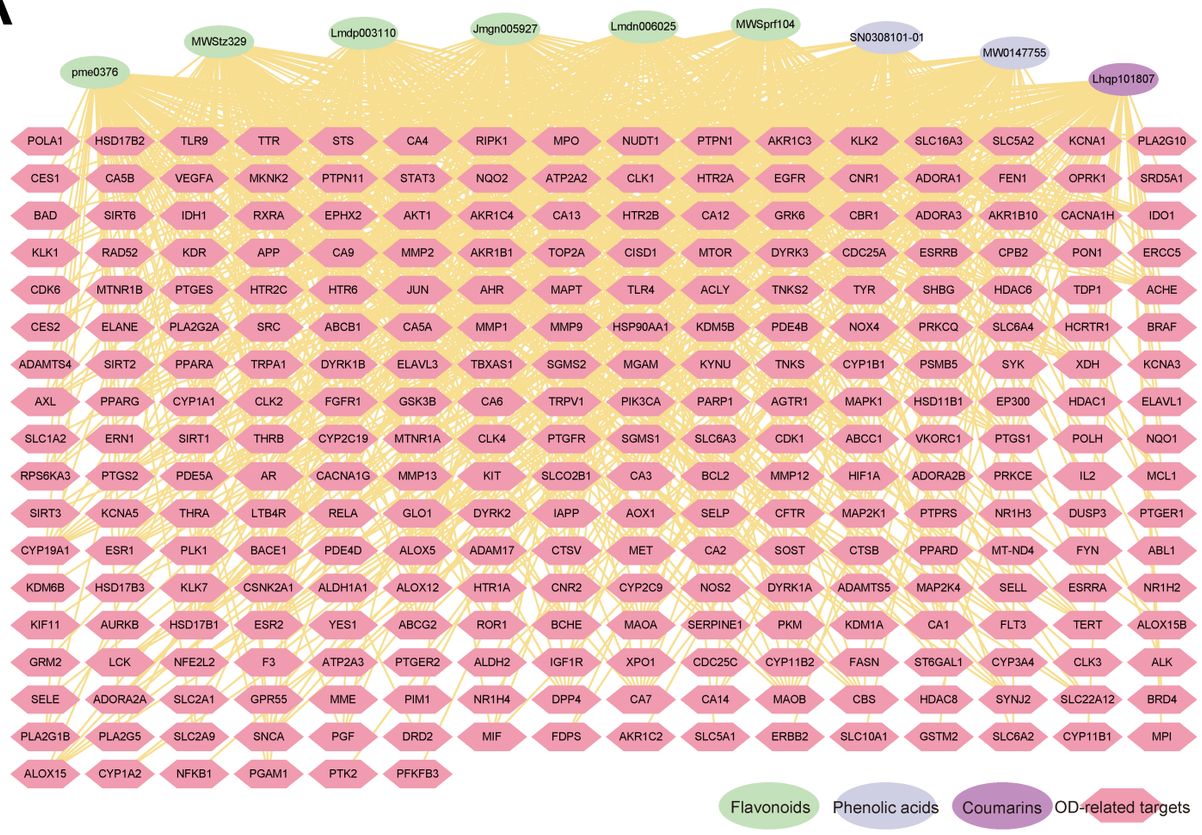
B


Number of metabolites
400
350
300
250
200
150
100
50
0
blue
greenyellow
black
pink
magenta
yellow
Class
Quinones
Steroids
Alcohol and amines
Benzenoids
Organoheterocyclic compounds
Amino acids and derivatives
Alkaloids and derivatives
Terpenoids
Organic acids and derivatives
Phenols
Others
Nucleotides and derivatives
Lipids and lipid-like molecules

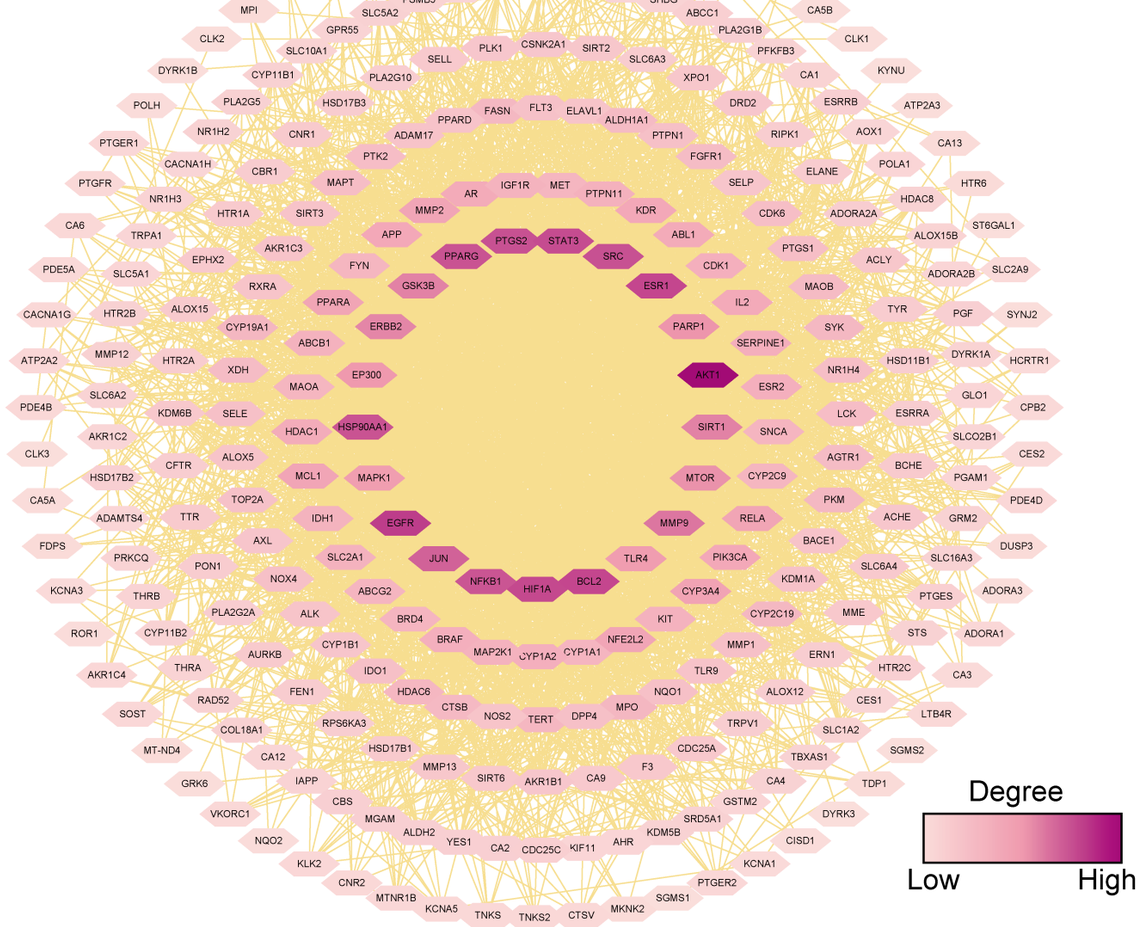
C


FRAP
ABTS
DPPH
Zmhn002173
Lmsn005161
Labn004865
Lmdp003110
mws0072
C00009195
SN0373390-02
MWStz521
tcm03_000539
Lmtn002796
CNP0131079
CNP0279684
Lmmn004625
LTS0147300
SN0471863-01
mws1454
CNP0159414
LTS0195446
CNP0111372
Lmsn004970
CNP0365370
SN0123518-01
MWSprf104
C00014876
MW0149539
Lmmn003663
C00008919
Wabn003563
PI0210397
SN0424066-01
Zbfn004208
LTS0064365
Lmjp002596
pme0376
SN0149495-01
C00009204
Lmnn002886
Jmgn005927
Lmsn003582
Wasn004683
Lhqp101807
PI0183181
C00014113
CNP0260164
SN0292958
SN0219694-01
Lmsn004090
Lmdn006025
MEDL01929
PI0011125
MW0148141
Ladp005021
PI0162262
PI0193414
Hmln002100
MW0147755
SN0097379
SN0283978
Lmhn002629
pma0795
MWSmce248
SN0308101-01
Lmsn003628
Lmyn005006
MWStz329
SN0183746-01
HJN078
Lahp003408
C00057630
LTS0029680
SN0295775-01
Hmln002199
Lmfn004093
Cmxn004016
SN0118300
Flavonoids
Phenolic acids
Tannins
Lignans
Stilbenes
Coumarins
Antioxidant-related indicators

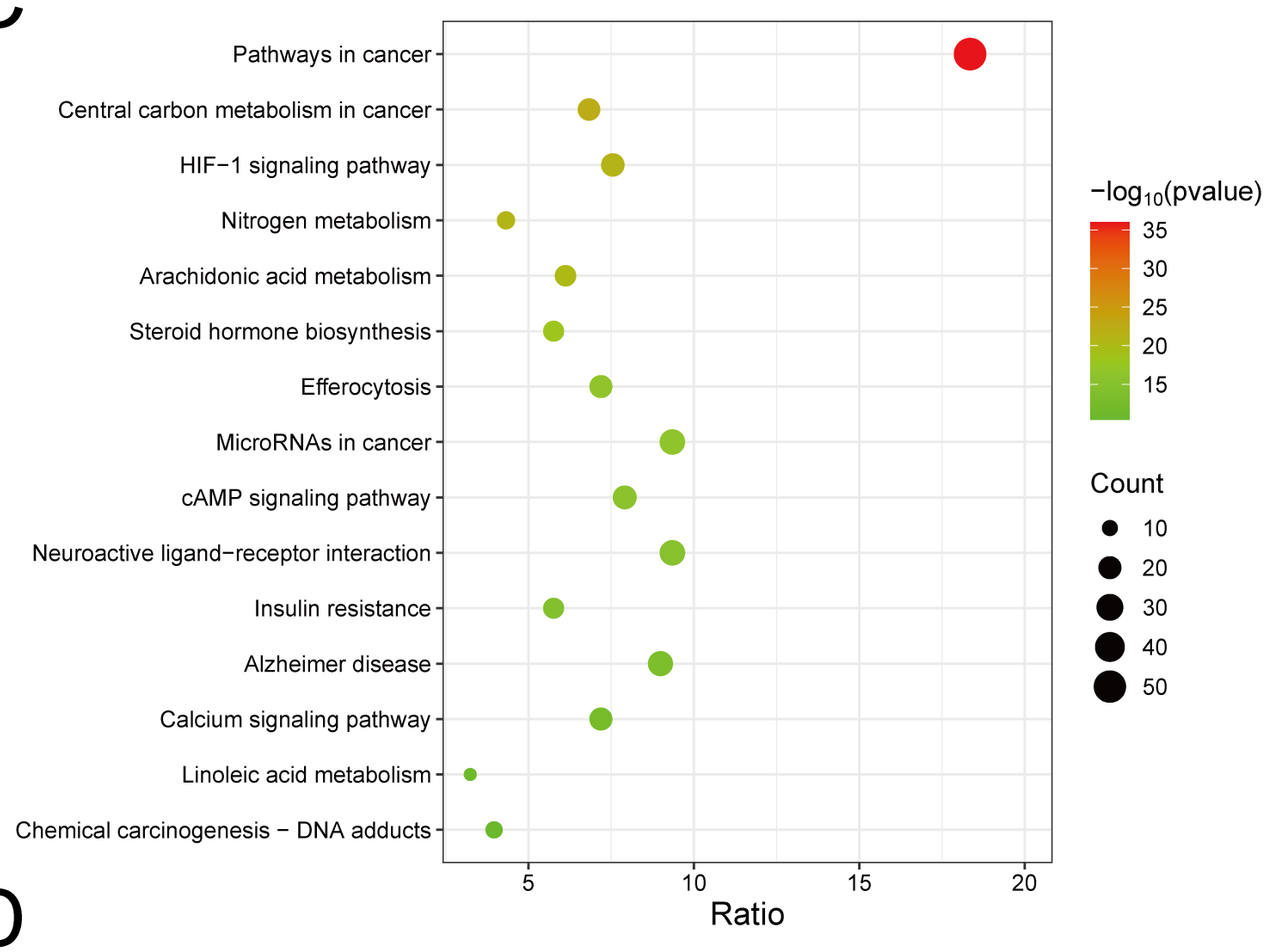
A


pme0376
MWStz329
Lmdp003110
Jmgn005927
Lmdn006025
MWSprf104
SN0308101-01
MW0147755
Lhqp101807
Flavonoids
Phenolic acids
Coumarins
OD-related targets

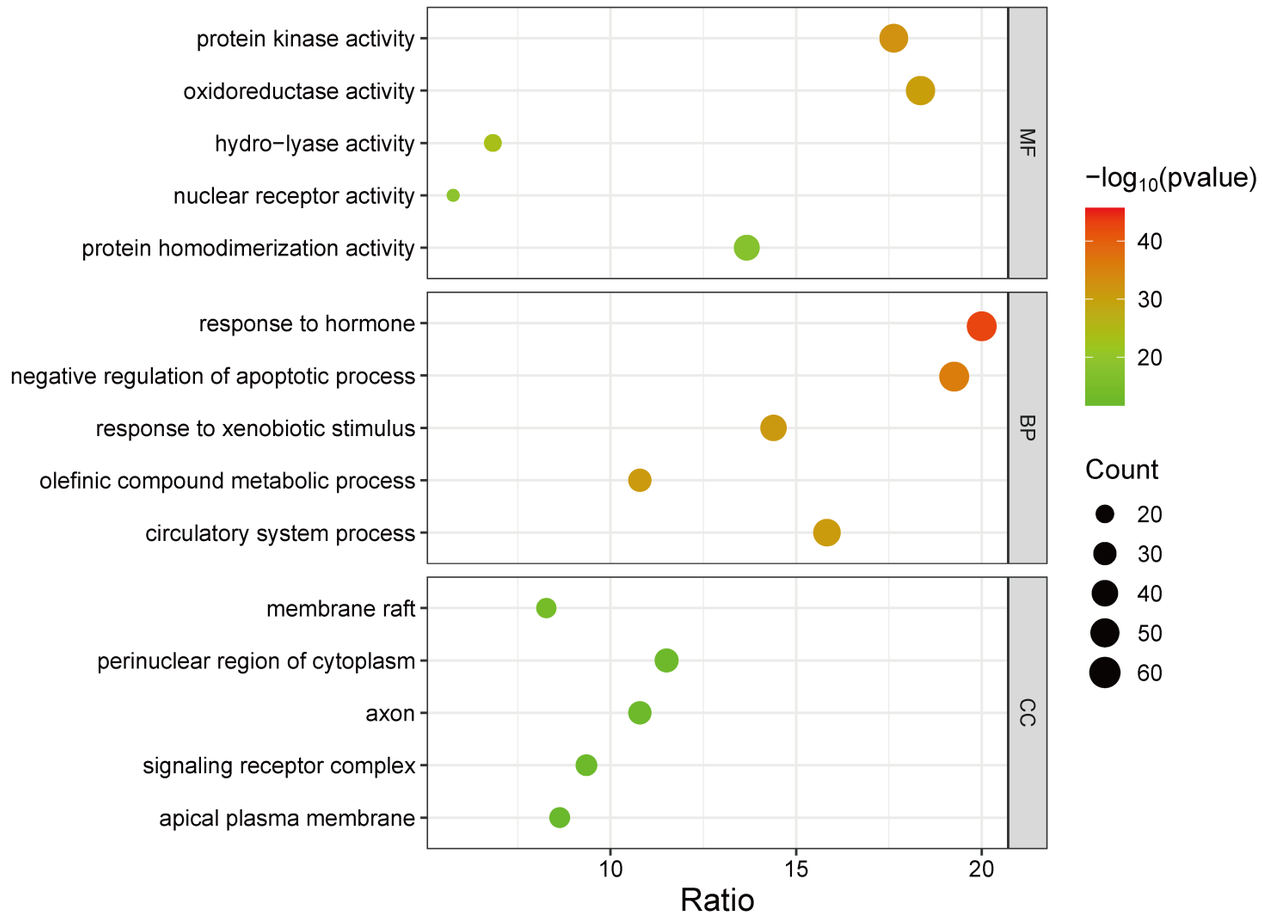
B


Degree
Low
High

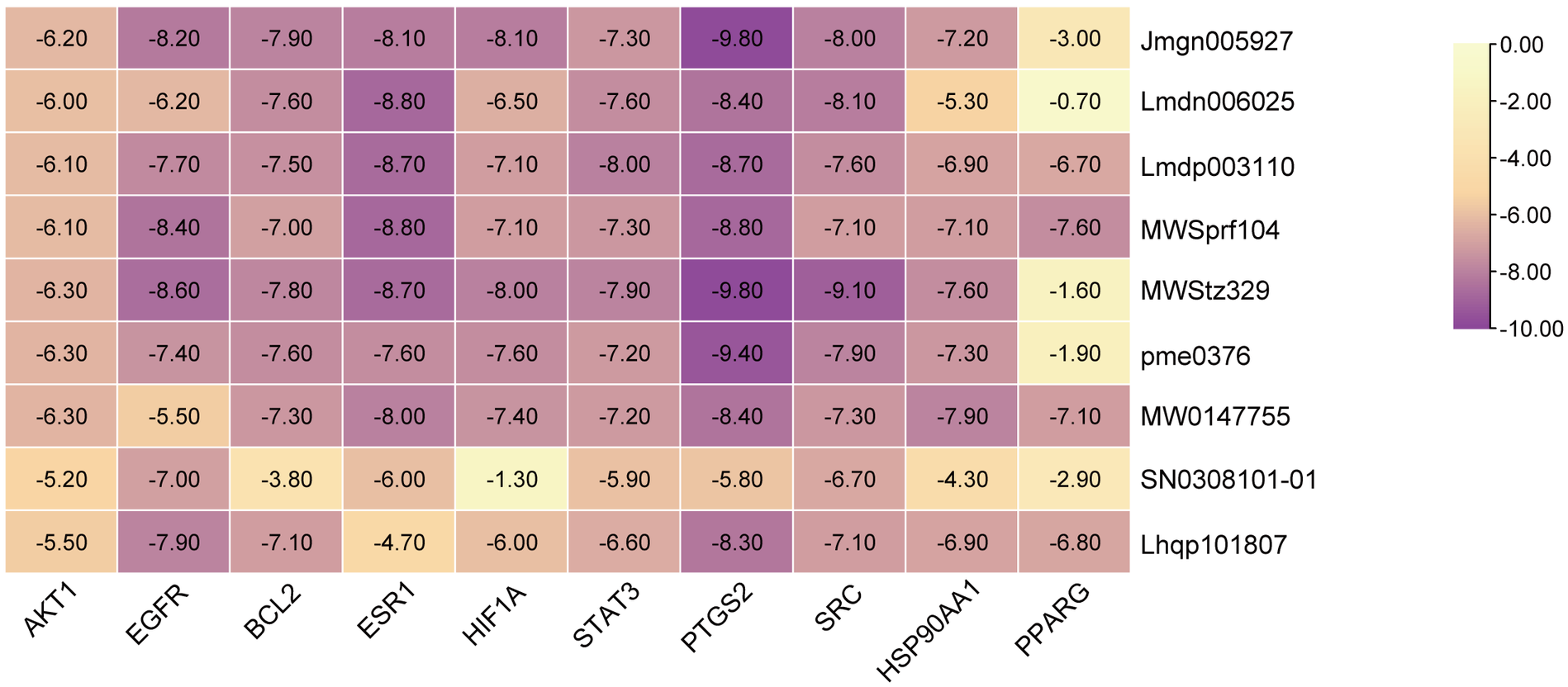
C


Pathways in cancer
Central carbon metabolism in cancer
HIF−1 signaling pathway
Nitrogen metabolism
Arachidonic acid metabolism
Steroid hormone biosynthesis
Efferocytosis
MicroRNAs in cancer
cAMP signaling pathway
Neuroactive ligand−receptor interaction
Insulin resistance
Alzheimer disease
Calcium signaling pathway
Linoleic acid metabolism
Chemical carcinogenesis − DNA adducts
5
10
15
20
Ratio
−log10(pvalue)
35
30
25
20
15
Count
10
20
30
40
50

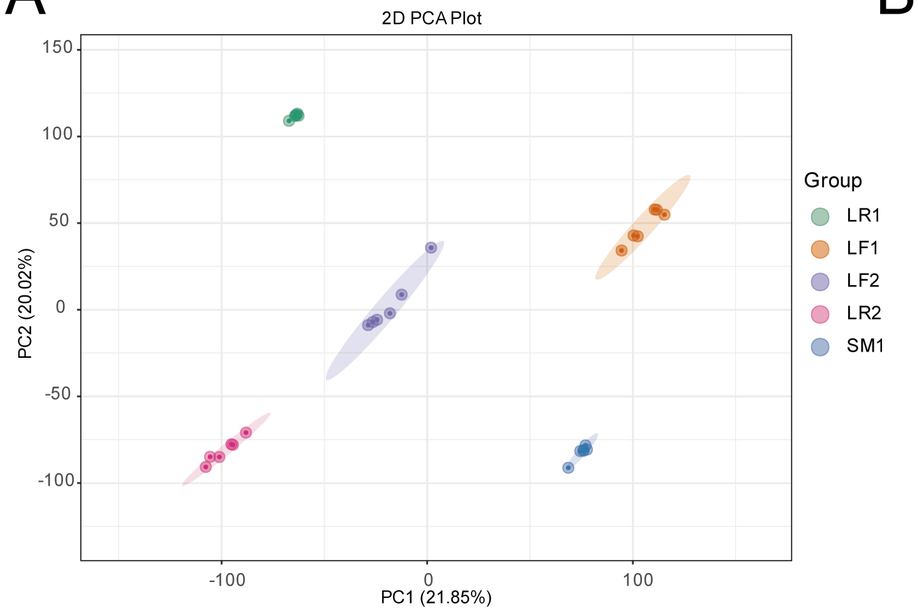
D


protein kinase activity
oxidoreductase activity
hydro−lyase activity
nuclear receptor activity
protein homodimerization activity
MF
response to hormone
negative regulation of apoptotic process
response to xenobiotic stimulus
olefinic compound metabolic process
circulatory system process
BP
membrane raft
perinuclear region of cytoplasm
axon
signaling receptor complex
apical plasma membrane
CC
10
15
20
Ratio
−log10(pvalue)
40
30
20
Count
20
30
40
50
60

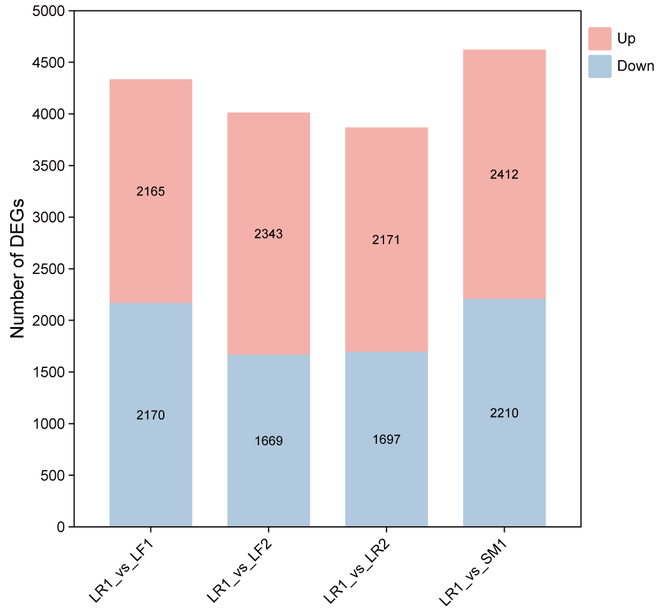
E


-6.20 -8.20 -7.90 -8.10 -8.10 -7.30 -9.80 -8.00 -7.20 -3.00 Jmgn005927
-6.00 -6.20 -7.60 -8.80 -6.50 -7.60 -8.40 -8.10 -5.30 -0.70 Lmdn006025
-6.10 -7.70 -7.50 -8.70 -7.10 -8.00 -8.70 -7.60 -6.90 -6.70 Lmdp003110
-6.10 -8.40 -7.00 -8.80 -7.10 -7.30 -8.80 -7.10 -7.10 -7.60 MWSprf104
-6.30 -8.60 -7.80 -8.70 -8.00 -7.90 -9.80 -9.10 -7.60 -1.60 MWStz329
-6.30 -7.40 -7.60 -7.60 -7.60 -7.20 -9.40 -7.90 -7.30 -1.90 pme0376
-6.30 -5.50 -7.30 -8.00 -7.40 -7.20 -8.40 -7.30 -7.90 -7.10 MW0147755
-5.20 -7.00 -3.80 -6.00 -1.30 -5.90 -5.80 -6.70 -4.30 -2.90 SN0308101-01
-5.50 -7.90 -7.10 -4.70 -6.00 -6.60 -8.30 -7.10 -6.90 -6.80 Lhqp101807
AKT1
EGFR
BCL2
ESR1
HIF1A
STAT3
PTGS2
SRC
HSP90AA1
PPARG
0.00
-2.00
-4.00
-6.00
-8.00
-10.00

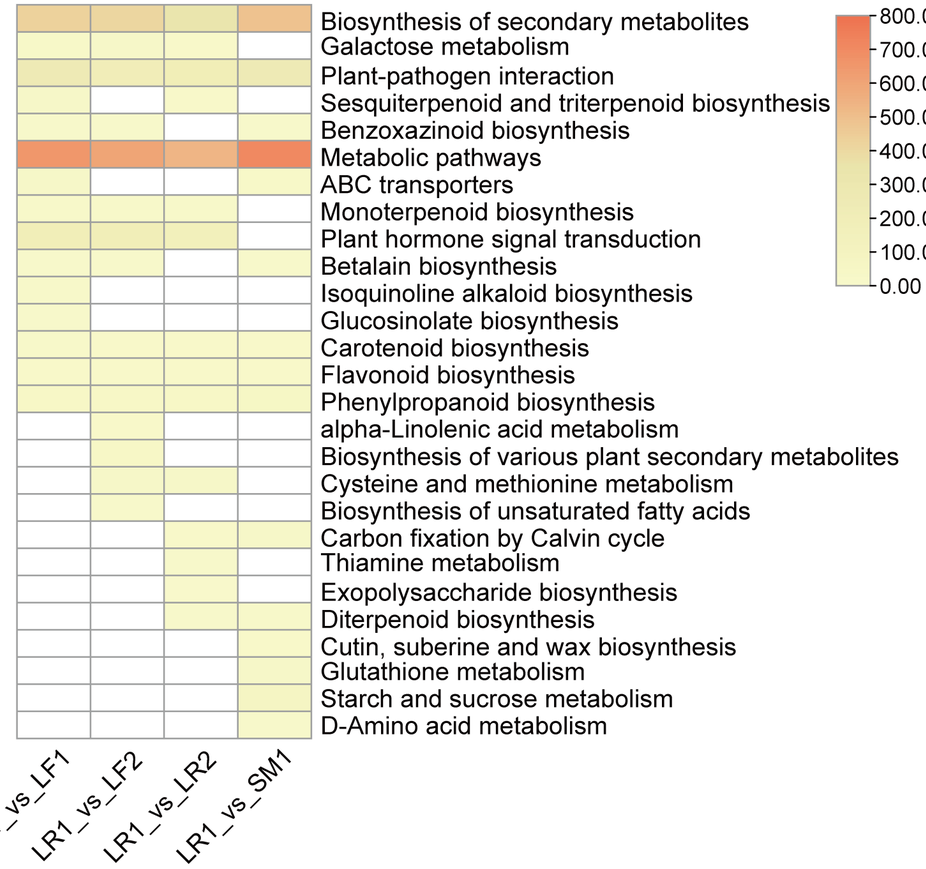
A


2D PCA Plot
PC2 (20.02%)
PC1 (21.85%)
Group
LR1
LF1
LF2
LR2
SM1

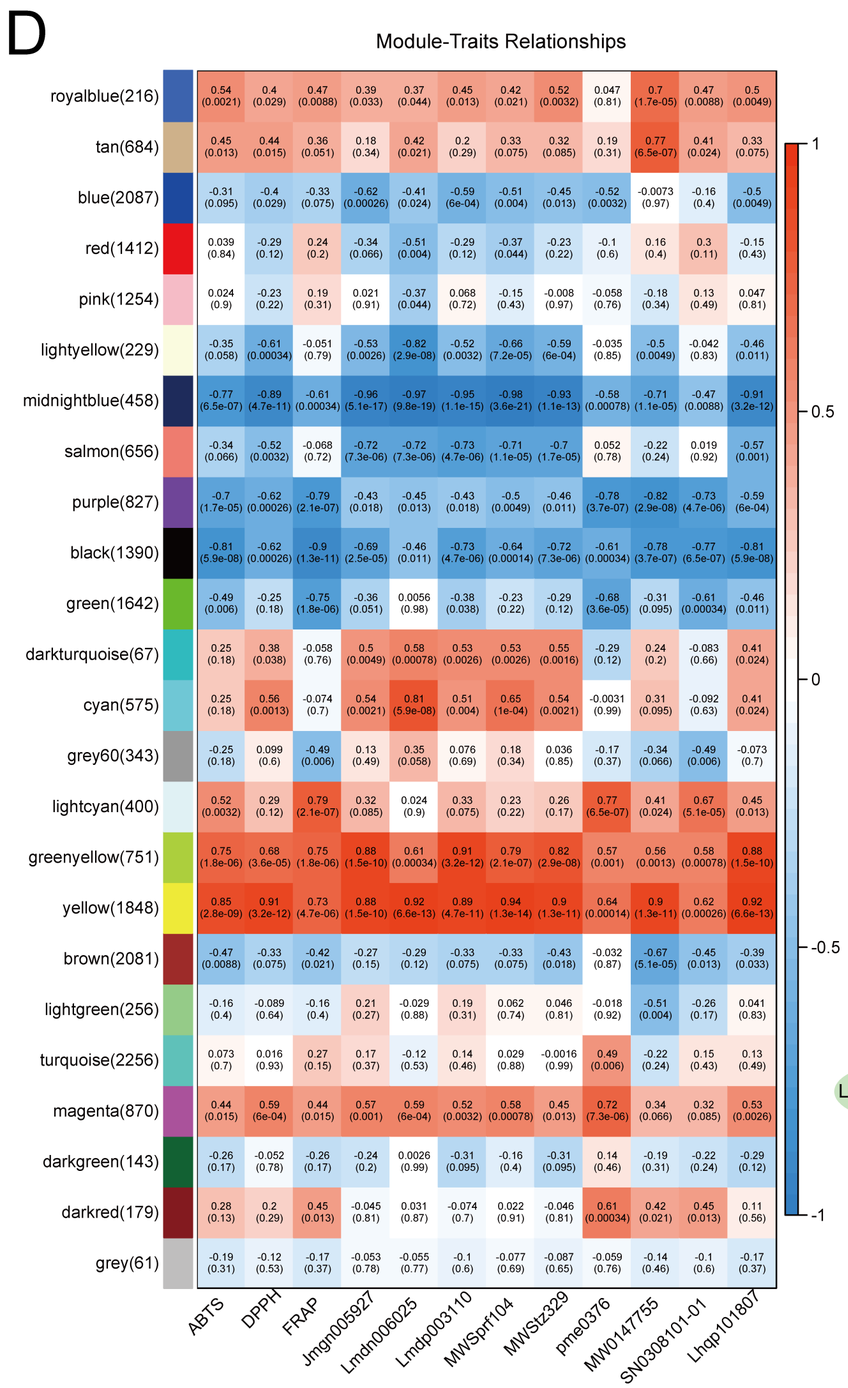
B


Number of DEGs
Up
Down
2165
2170
2343
1669
2171
1697
2412
2210
LR1_vs_LF1
LR1_vs_LF2
LR1_vs_LR2
LR1_vs_SM1

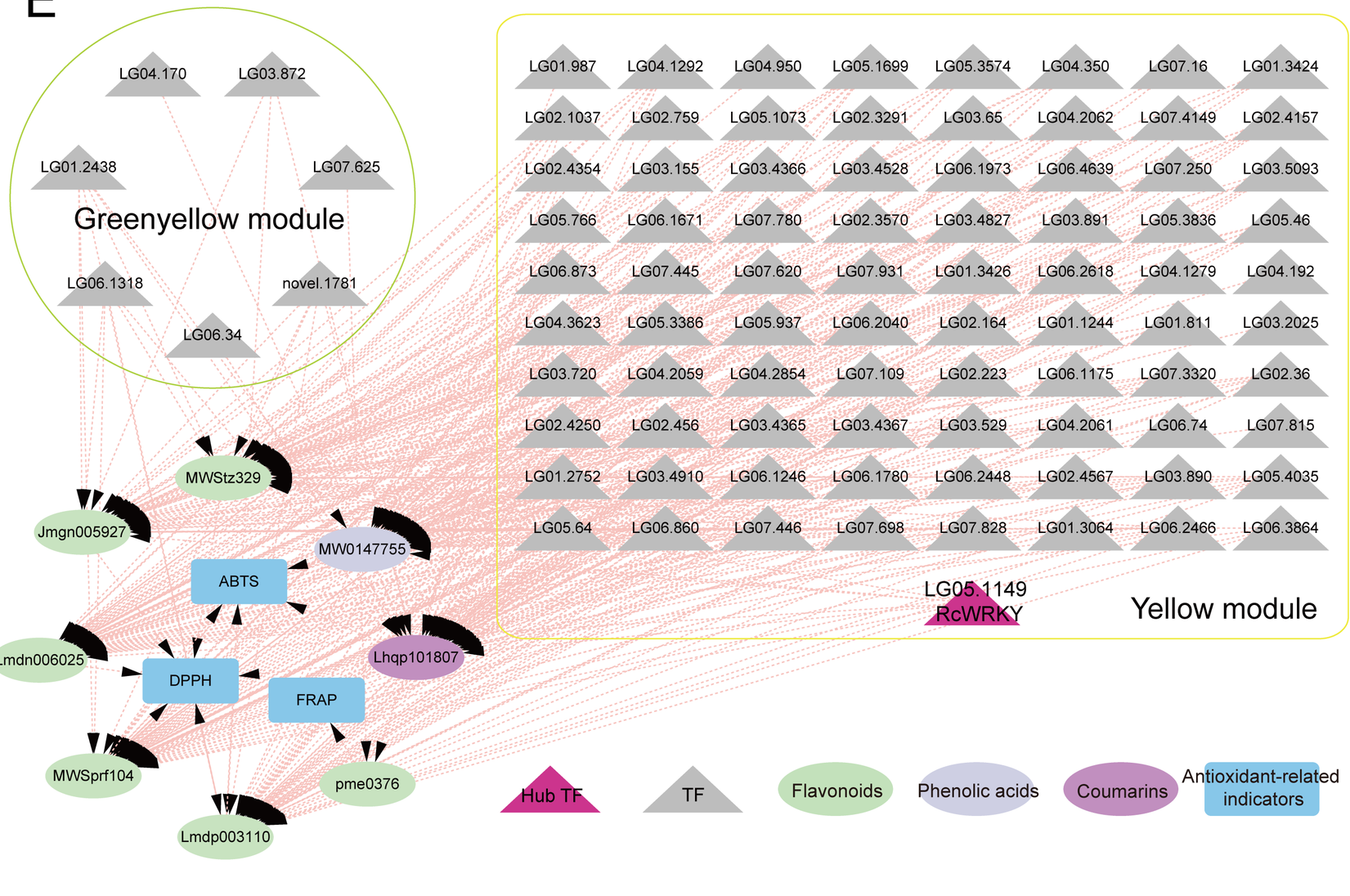
C


Biosynthesis of secondary metabolites
Galactose metabolism
Plant-pathogen interaction
Sesquiterpenoid and triterpenoid biosynthesis
Benzoxazinoid biosynthesis
Metabolic pathways
ABC transporters
Monoterpenoid biosynthesis
Plant hormone signal transduction
Betalain biosynthesis
Isoquinoline alkaloid biosynthesis
Glucosinolate biosynthesis
Carotenoid biosynthesis
Flavonoid biosynthesis
Phenylpropanoid biosynthesis
alpha-Linolenic acid metabolism
Biosynthesis of various plant secondary metabolites
Cysteine and methionine metabolism
Biosynthesis of unsaturated fatty acids
Carbon fixation by Calvin cycle
Thiamine metabolism
Exopolysaccharide biosynthesis
Diterpenoid biosynthesis
Cutin, suberine and wax biosynthesis
Glutathione metabolism
Starch and sucrose metabolism
D-Amino acid metabolism
800.00
700.00
600.00
500.00
400.00
300.00
200.00
100.00
0.00
LR1_vs_LF1
LR1_vs_LF2
LR1_vs_LR2
LR1_vs_SM1

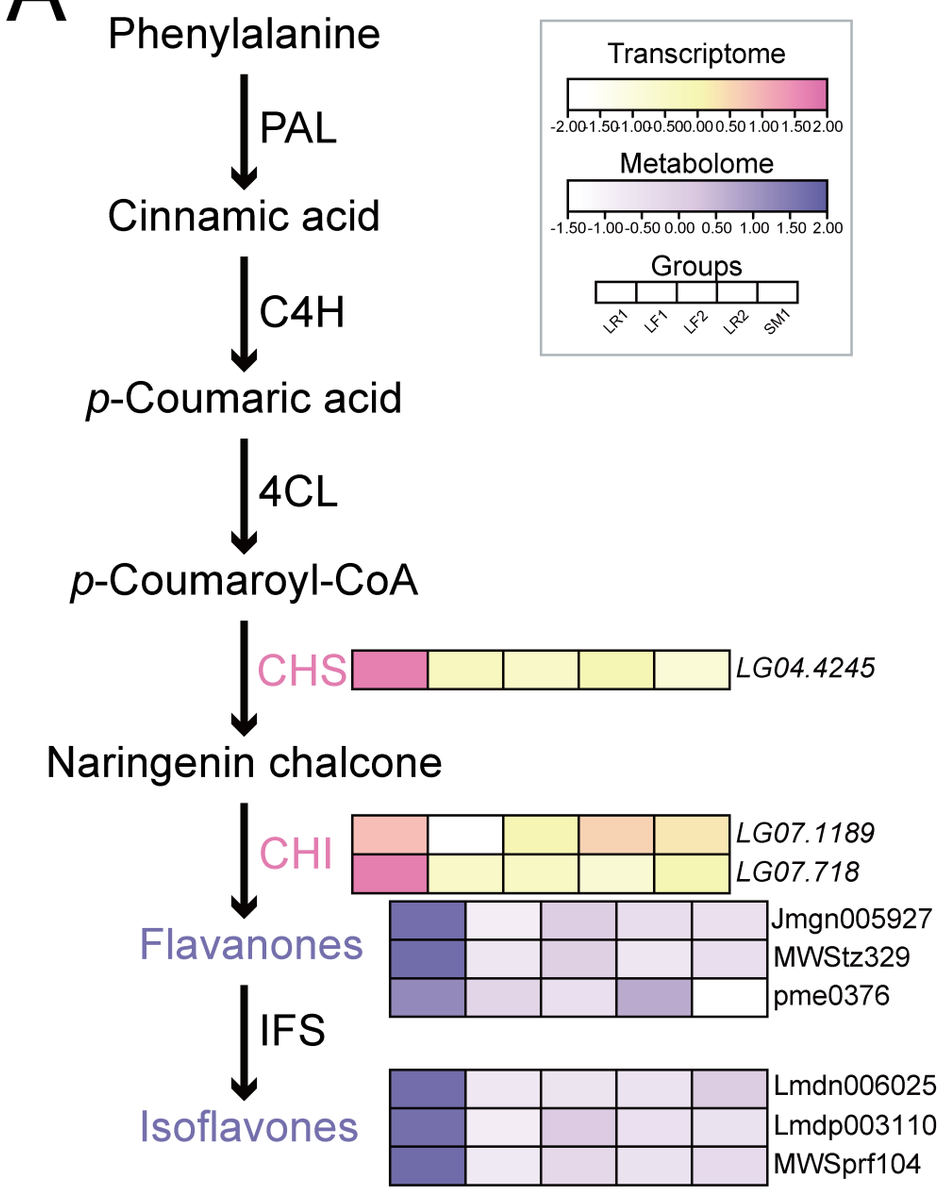
D


Module-Traits Relationships
royalblue(216) 0.54 (0.0021) 0.4 (0.029) 0.47 (0.0088) 0.39 (0.033) 0.37 (0.044) 0.45 (0.013) 0.42 (0.021) 0.52 (0.0032) 0.047 (0.81) 0.7 (1.7e-05) 0.47 (0.0088) 0.5 (0.0049)
tan(684) 0.45 (0.013) 0.44 (0.015) 0.36 (0.051) 0.18 (0.34) 0.42 (0.021) 0.2 (0.29) 0.33 (0.075) 0.32 (0.085) 0.19 (0.31) 0.77 (6.5e-07) 0.41 (0.024) 0.33 (0.075)
blue(2087) -0.31 (0.095) -0.4 (0.029) -0.33 (0.075) -0.62 (0.00026) -0.41 (0.024) -0.59 (6e-04) -0.51 (0.004) -0.45 (0.013) -0.52 (0.0032) -0.0073 (0.97) -0.16 (0.4) -0.5 (0.0049)
red(1412) 0.039 (0.84) -0.29 (0.12) 0.24 (0.2) -0.34 (0.066) -0.51 (0.004) -0.29 (0.12) -0.37 (0.044) -0.23 (0.22) -0.1 (0.6) 0.16 (0.4) 0.3 (0.11) -0.15 (0.43)
pink(1254) 0.024 (0.9) -0.23 (0.22) 0.19 (0.31) 0.021 (0.91) -0.37 (0.044) 0.068 (0.72) -0.15 (0.43) -0.008 (0.97) -0.058 (0.76) -0.18 (0.34) 0.13 (0.49) 0.047 (0.81)
lightyellow(229) -0.35 (0.058) -0.61 (0.00034) -0.051 (0.79) -0.53 (0.0026) -0.82 (2.9e-08) -0.52 (0.0032) -0.66 (7.2e-05) -0.59 (6e-04) -0.035 (0.85) -0.5 (0.0049) -0.042 (0.83) -0.46 (0.011)
midnightblue(458) -0.77 (6.5e-07) -0.89 (4.7e-11) -0.61 (0.00034) -0.96 (5.1e-17) -0.97 (9.8e-19) -0.95 (1.1e-15) -0.98 (3.6e-21) -0.93 (1.1e-13) -0.58 (0.00078) -0.71 (1.1e-05) -0.47 (0.0088) -0.91 (3.2e-12)
salmon(656) -0.34 (0.066) -0.52 (0.0032) -0.068 (0.72) -0.72 (7.3e-06) -0.72 (7.3e-06) -0.73 (4.7e-06) -0.71 (1.1e-05) -0.7 (1.7e-05) 0.052 (0.78) -0.22 (0.24) 0.019 (0.92) -0.57 (0.001)
purple(827) -0.7 (1.7e-05) -0.62 (0.00026) -0.79 (2.1e-07) -0.43 (0.018) -0.45 (0.013) -0.43 (0.018) -0.5 (0.0049) -0.46 (0.011) -0.78 (3.7e-07) -0.82 (2.9e-08) -0.73 (4.7e-06) -0.59 (6e-04)
black(1390) -0.81 (5.9e-08) -0.62 (0.00026) -0.9 (1.3e-11) -0.69 (2.5e-05) -0.46 (0.011) -0.73 (4.7e-06) -0.64 (0.00014) -0.72 (7.3e-06) -0.61 (0.00034) -0.78 (3.7e-07) -0.77 (6.5e-07) -0.81 (5.9e-08)
green(1642) -0.49 (0.006) -0.25 (0.18) -0.75 (1.8e-06) -0.36 (0.051) 0.0056 (0.98) -0.38 (0.038) -0.23 (0.22) -0.29 (0.12) -0.68 (3.6e-05) -0.31 (0.095) -0.61 (0.00034) -0.46 (0.011)
darkturquoise(67) 0.25 (0.18) 0.38 (0.038) -0.058 (0.76) 0.5 (0.0049) 0.58 (0.00078) 0.53 (0.0026) 0.53 (0.0026) 0.55 (0.0016) -0.29 (0.12) 0.24 (0.2) -0.083 (0.66) 0.41 (0.024)
cyan(575) 0.25 (0.18) 0.56 (0.0013) -0.074 (0.7) 0.54 (0.0021) 0.81 (5.9e-08) 0.51 (0.004) 0.65 (1e-04) 0.54 (0.0021) -0.0031 (0.99) 0.31 (0.095) -0.092 (0.63) 0.41 (0.024)
grey60(343) -0.25 (0.18) 0.099 (0.6) -0.49 (0.006) 0.13 (0.49) 0.35 (0.058) 0.076 (0.69) 0.18 (0.34) 0.036 (0.85) -0.17 (0.37) -0.34 (0.066) -0.49 (0.006) -0.073 (0.7)
lightcyan(400) 0.52 (0.0032) 0.29 (0.12) 0.79 (2.1e-07) 0.32 (0.085) 0.024 (0.9) 0.33 (0.075) 0.23 (0.22) 0.26 (0.17) 0.77 (6.5e-07) 0.41 (0.024) 0.67 (5.1e-05) 0.45 (0.013)
greenyellow(751) 0.75 (1.8e-06) 0.68 (3.6e-05) 0.75 (1.8e-06) 0.88 (1.5e-10) 0.61 (0.00034) 0.91 (3.2e-12) 0.79 (2.1e-07) 0.82 (2.9e-08) 0.57 (0.001) 0.56 (0.0013) 0.58 (0.00078) 0.88 (1.5e-10)
yellow(1848) 0.85 (2.8e-09) 0.91 (3.2e-12) 0.73 (4.7e-06) 0.88 (1.5e-10) 0.92 (6.6e-13) 0.89 (4.7e-11) 0.94 (1.3e-14) 0.9 (1.3e-11) 0.64 (0.00014) 0.9 (1.3e-11) 0.62 (0.00026) 0.92 (6.6e-13)
brown(2081) -0.47 (0.0088) -0.33 (0.075) -0.42 (0.021) -0.27 (0.15) -0.29 (0.12) -0.33 (0.075) -0.33 (0.075) -0.43 (0.018) -0.032 (0.87) -0.67 (5.1e-05) -0.45 (0.013) -0.39 (0.033)
lightgreen(256) -0.16 (0.4) -0.089 (0.64) -0.16 (0.4) 0.21 (0.27) -0.029 (0.88) 0.19 (0.31) 0.062 (0.74) 0.046 (0.81) -0.018 (0.92) -0.51 (0.004) -0.26 (0.17) 0.041 (0.83)
turquoise(2256) 0.073 (0.7) 0.016 (0.93) 0.27 (0.15) 0.17 (0.37) -0.12 (0.53) 0.14 (0.46) 0.029 (0.88) -0.0016 (0.99) 0.49 (0.006) -0.22 (0.24) 0.15 (0.43) 0.13 (0.49)
magenta(870) 0.44 (0.015) 0.59 (6e-04) 0.44 (0.015) 0.57 (0.001) 0.59 (6e-04) 0.52 (0.0032) 0.58 (0.00078) 0.45 (0.013) 0.72 (7.3e-06) 0.34 (0.066) 0.32 (0.085) 0.53 (0.0026)
darkgreen(143) -0.26 (0.17) -0.052 (0.78) -0.26 (0.17) -0.24 (0.2) 0.0026 (0.99) -0.31 (0.095) -0.16 (0.4) -0.31 (0.095) 0.14 (0.46) -0.19 (0.31) -0.22 (0.24) -0.29 (0.12)
darkred(179) 0.28 (0.13) 0.2 (0.29) 0.45 (0.013) -0.045 (0.81) 0.031 (0.87) -0.074 (0.7) 0.022 (0.91) -0.046 (0.81) 0.61 (0.00034) 0.42 (0.021) 0.45 (0.013) 0.11 (0.56)
grey(61) -0.19 (0.31) -0.12 (0.53) -0.17 (0.37) -0.053 (0.78) -0.055 (0.77) -0.1 (0.6) -0.077 (0.69) -0.087 (0.65) -0.059 (0.76) -0.14 (0.46) -0.1 (0.6) -0.17 (0.37)
1
0.5
0
-0.5
-1
ABTS
DPPH
FRAP
Jmgn005927
Lmdn006025
Lmdp003110
MWSprf104
MWStz329
pme0376
MW0147755
SN0308101-01
Lhqp101807

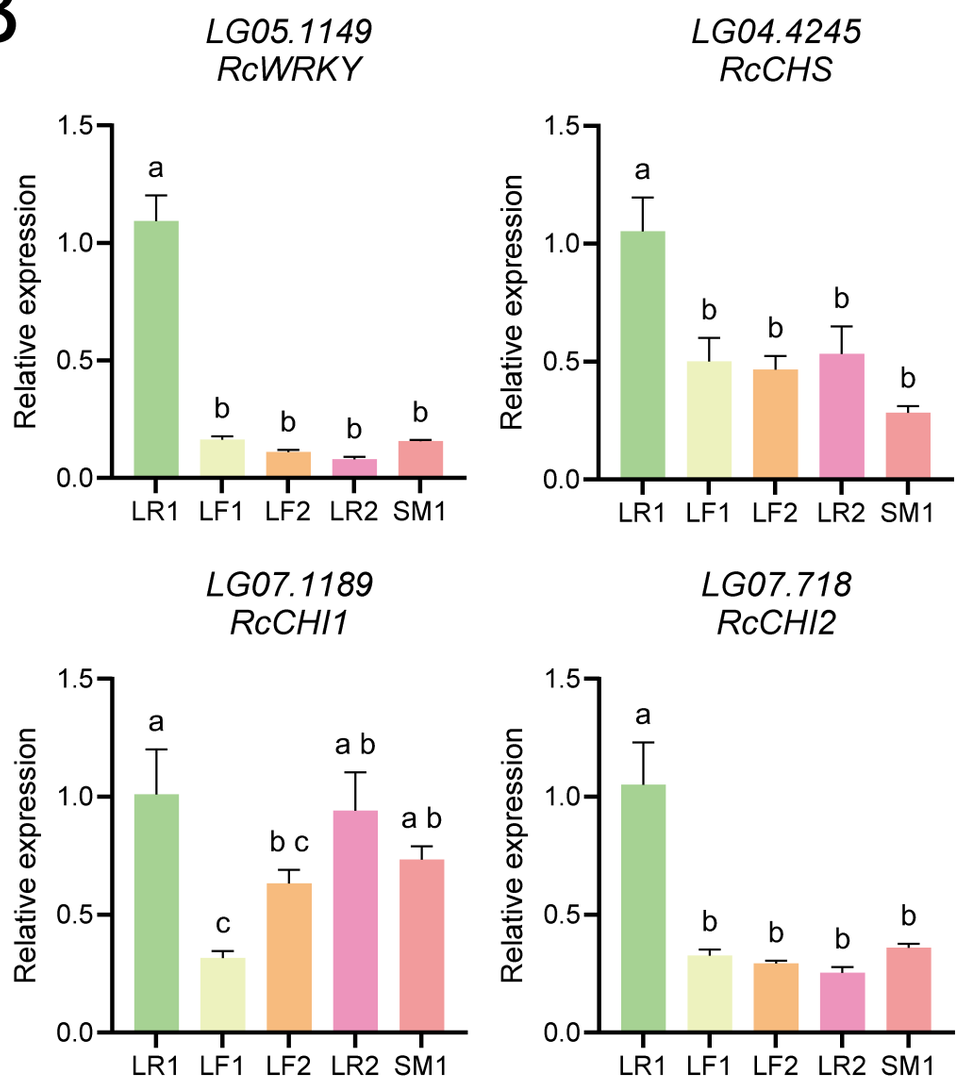
E


LG04.170
LG03.872
LG01.2438
LG07.625
Greenyellow module
LG06.1318
novel.1781
LG06.34
MWStz329
Jmgn005927
MW0147755
ABTS
Lmdn006025
Lhqp101807
DPPH
FRAP
MWSprf104
pme0376
Lmdp003110
LG01.987 LG04.1292 LG04.950 LG05.1699 LG05.3574 LG04.350 LG07.16 LG01.3424
LG02.1037 LG02.759 LG05.1073 LG02.3291 LG03.65 LG04.2062 LG07.4149 LG02.4157
LG02.4354 LG03.155 LG03.4366 LG03.4528 LG06.1973 LG06.4639 LG07.250 LG03.5093
LG05.766 LG06.1671 LG07.780 LG02.3570 LG03.4827 LG03.891 LG05.3836 LG05.46
LG06.873 LG07.445 LG07.620 LG07.931 LG01.3426 LG06.2618 LG04.1279 LG04.192
LG04.3623 LG05.3386 LG05.937 LG06.2040 LG02.164 LG01.1244 LG01.811 LG03.2025
LG03.720 LG04.2059 LG04.2854 LG07.109 LG02.223 LG06.1175 LG07.3320 LG02.36
LG02.4250 LG02.456 LG03.4365 LG03.4367 LG03.529 LG04.2061 LG06.74 LG07.815
LG01.2752 LG03.4910 LG06.1246 LG06.1780 LG06.2448 LG02.4567 LG03.890 LG05.4035
LG05.64 LG06.860 LG07.446 LG07.698 LG07.828 LG01.3064 LG06.2466 LG06.3864
LG05.1149
RcWRKY
Yellow module
Hub TF
TF
Flavonoids
Phenolic acids
Coumarins
Antioxidant-related indicators

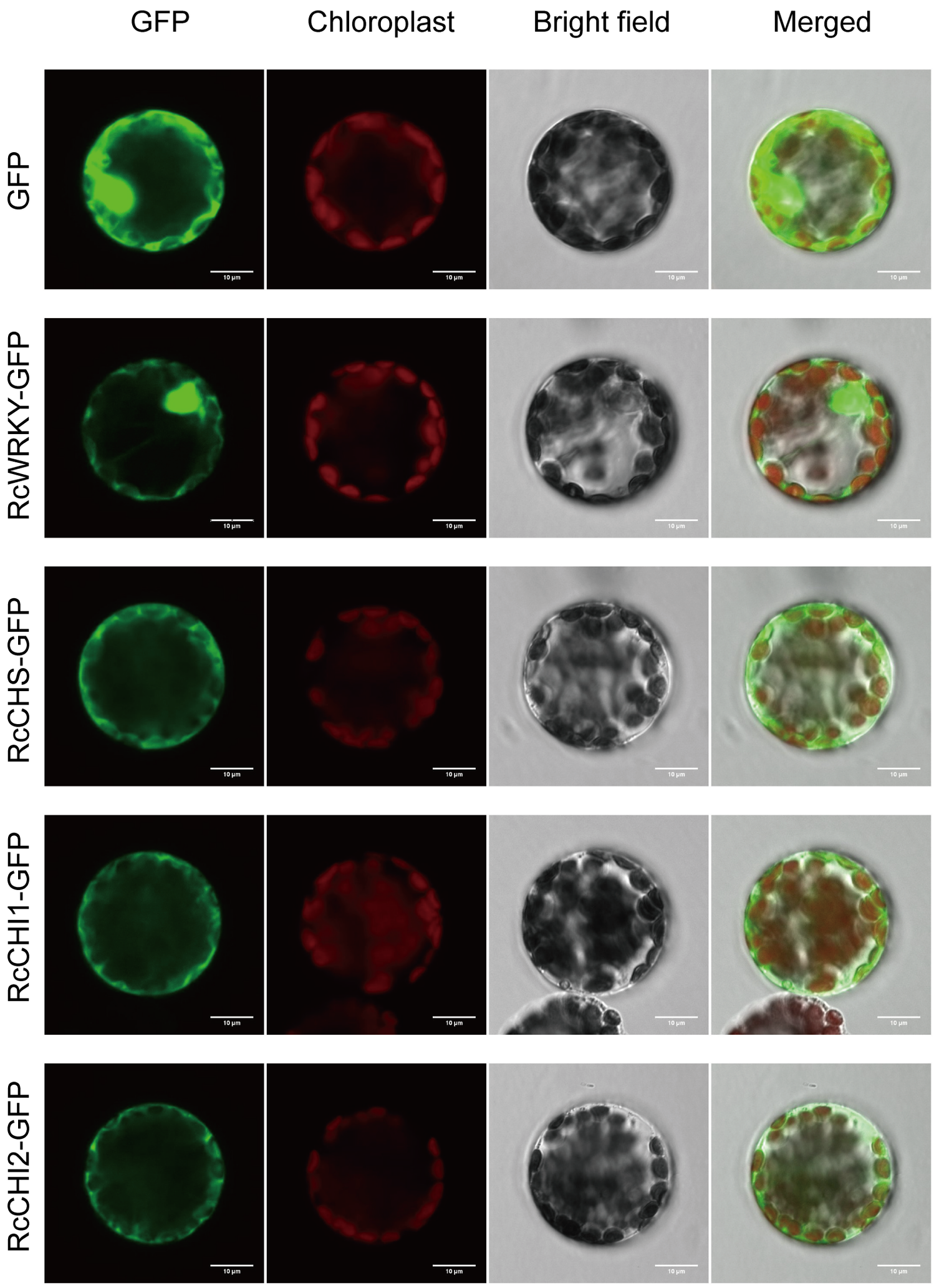
A

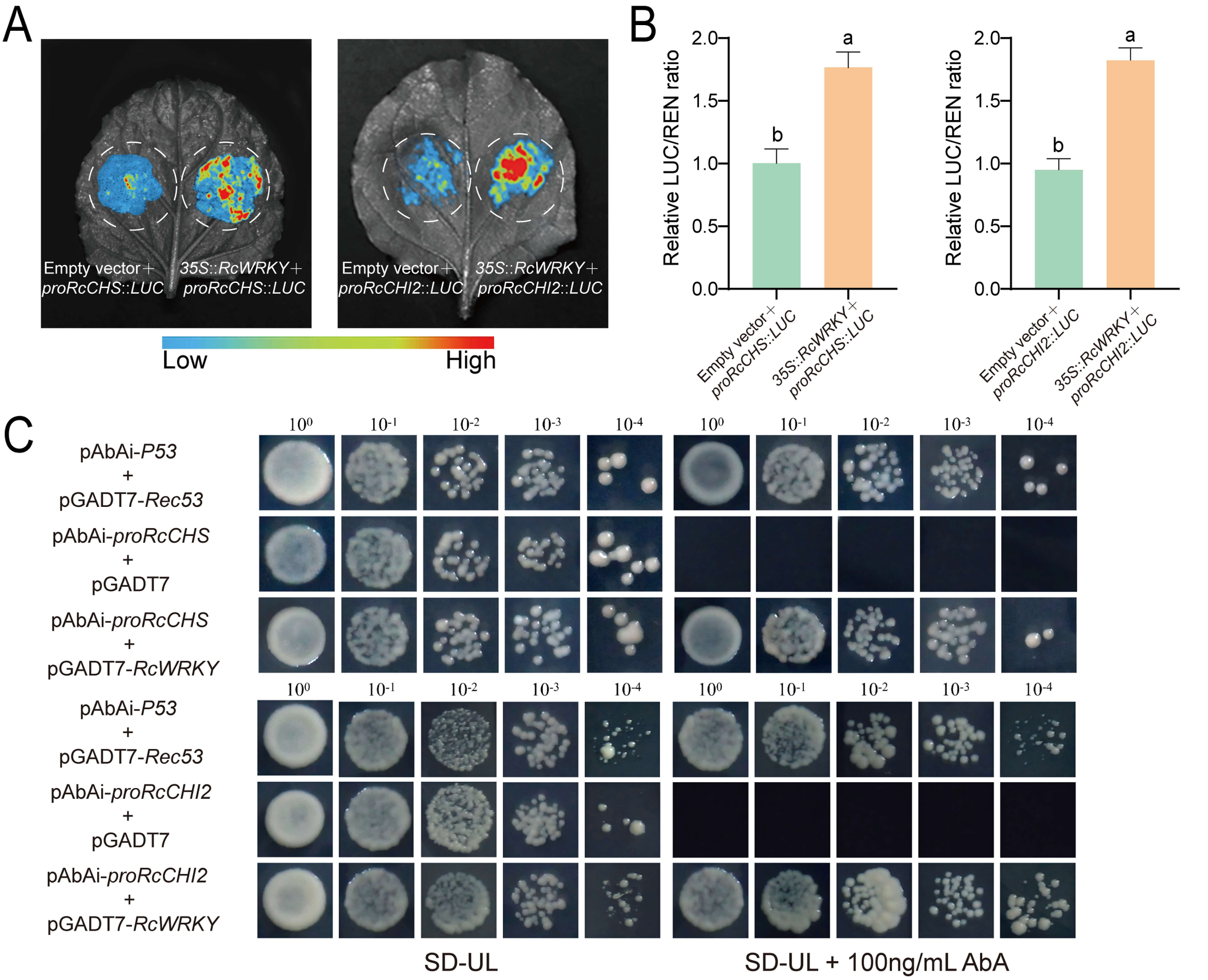

Phenylalanine
PAL
Cinnamic acid
C4H
p-Coumaric acid
4CL
p-Coumaroyl-CoA
CHS
LG04.4245
Naringenin chalcone
CHI
LG07.1189
LG07.718
Flavanones
Jmgn005927
MWStz329
pme0376
IFS
Isoflavones
Lmdn006025
Lmdp003110
MWSprf104
Transcriptome
-2.00 -1.50 -1.00 -0.50 0.00 0.50 1.00 1.50 2.00
Metabolome
-1.50 -1.00 -0.50 0.00 0.50 1.00 1.50 2.00
Groups
LR1 LF1 LF2 LR2 SM1

B


LG05.1149
RcWRKY
LG04.4245
RcCHS
LG07.1189
RcCHI1
LG07.718
RcCHI2
Relative expression
0.0
0.5
1.0
1.5
a
b
c
b c
a b
LR1 LF1 LF2 LR2 SM1

C


GFP
Chloroplast
Bright field
Merged
GFP
RcWRKY-GFP
RcCHS-GFP
RcCHI1-GFP
RcCHI2-GFP
10 μm


A
Empty vector+
proRcCHS::LUC
35S::RcWRKY+
proRcCHS::LUC
Empty vector+
proRcCHI2::LUC
35S::RcWRKY+
proRcCHI2::LUC
Low
High
B
Relative LUC/REN ratio
2.0
1.5
1.0
0.5
0.0
a
b
Empty vector+
proRcCHS::LUC
35S::RcWRKY+
proRcCHS::LUC
Relative LUC/REN ratio
2.0
1.5
1.0
0.5
0.0
a
b
Empty vector+
proRcCHI2::LUC
35S::RcWRKY+
proRcCHI2::LUC
C
pAbAi-P53
+
pGADT7-Rec53
pAbAi-proRcCHS
+
pGADT7
pAbAi-proRcCHS
+
pGADT7-RcWRKY
pAbAi-P53
+
pGADT7-Rec53
pAbAi-proRcCHI2
+
pGADT7
pAbAi-proRcCHI2
+
pGADT7-RcWRKY
10^0
10^-1
10^-2
10^-3
10^-4
SD-UL
SD-UL + 100ng/mL AbA

Supplementary Files

This is a list of supplementary files associated with this preprint. Click to download.

- SupplementaryTable.pdf